

# Energy evolution of the moments of the hadron distribution in QCD jets including NNLL resummation and NLO running-coupling corrections

Redamy Pérez-Ramos<sup>1,\*</sup> and David d’Enterria<sup>2,†</sup>

<sup>1</sup> *Department of Physics, University of Jyväskylä, P.O. Box 35 (YFL), F-40014 Jyväskylä, Finland*

<sup>2</sup> *CERN, PH Department, CH-1211 Geneva 23, Switzerland*

## Abstract

The moments of the single inclusive momentum distribution of hadrons in QCD jets, are studied in the next-to-modified-leading-log approximation (NMLLA) including next-to-leading-order (NLO) corrections to the  $\alpha_s$  strong coupling. The evolution equations are solved using a distorted Gaussian parametrisation, which successfully reproduces the spectrum of charged hadrons of jets measured in  $e^+e^-$  collisions. The energy dependencies of the maximum peak, multiplicity, width, kurtosis and skewness of the jet hadron distribution are computed analytically. Comparisons of all the existing jet data measured in  $e^+e^-$  collisions in the range  $\sqrt{s} \approx 2\text{--}200$  GeV to the NMLLA+NLO\* predictions allow one to extract a value of the QCD parameter  $\Lambda_{\text{QCD}}$ , and associated two-loop coupling constant at the Z resonance  $\alpha_s(m_Z^2) = 0.1195 \pm 0.0022$ , in excellent numerical agreement with the current world average obtained using other methods.

## Contents

<b>1</b>	<b>Introduction</b>	<b>2</b>
<b>2</b>	<b>Evolution equations for the low-<math>x</math> parton fragmentation functions</b>	<b>5</b>
<b>3</b>	<b>Evolution of the parton fragmentation functions at NMLLA +NLO*</b>	<b>8</b>
3.1	Anomalous dimension at NMLLA +NLO* . . . . .	8
3.2	Distorted Gaussian (DG) parametrisation for the fragmentation function . . . . .	10
3.3	Multiplicities for the single inclusive $D_g$ and $D_q$ distributions . . . . .	15
3.4	Limiting spectrum for the DG parametrisation . . . . .	17
3.5	Higher-order corrections for the DG limiting spectrum . . . . .	20
3.6	Other corrections: finite mass, number of active flavours, power terms, and $\Lambda_{\text{QCD}}$ rescaling	25
<b>4</b>	<b>Extraction of <math>\alpha_s</math> from the evolution of the distribution of hadrons in jets in <math>e^+e^-</math> collisions</b>	<b>26</b>
<b>5</b>	<b>Conclusions and outlook</b>	<b>33</b>
<b>A</b>	<b>Mellin-transformed splitting functions</b>	<b>34</b>
<b>B</b>	<b>NMLLA+NLO* moments <math>K_n</math> of the distorted Gaussian</b>	<b>35</b>
<b>C</b>	<b>Higher-order corrections to the moments of the distorted Gaussian</b>	<b>36</b>

---

\* e-mail: redamy.perez@uv.es

† e-mail: dde@cern.ch

# 1 Introduction

One of the most ubiquitous manifestations of the fundamental degrees of freedom of Quantum Chromodynamics (QCD), quark and gluons, are the collimated bunches of hadrons (“jets”) produced in high-energy particle collisions. The evolution of a parton into a final distribution of hadrons is driven by perturbative dynamics dominated by soft and collinear gluon bremsstrahlung [1, 2] followed by the final conversion of the radiated partons into hadrons at non-perturbative scales approaching  $\Lambda_{\text{QCD}} \approx 0.2$  GeV. The quantitative description of the distribution of hadrons of type  $h$  in a jet is encoded in a (dimensionless) fragmentation function (FF) which can be experimentally obtained, e.g. in  $e^+e^-$  collisions at c.m. energy  $\sqrt{s}$ , via

$$D^h(\ln(1/x), s) = \frac{d\sigma(ee \rightarrow hX)}{\sigma_{\text{tot}} d \ln(1/x)},$$

where  $x = 2p_h/\sqrt{s}$  is the scaled momentum of hadron  $h$ , and  $\sigma_{\text{tot}}$  the total  $e^+e^-$  hadronic cross section. Its integral over  $x$  gives the average hadron multiplicity in jets. Writing the FF as a function of the (log of the) inverse of  $x$ ,  $\xi = \ln(1/x)$ , emphasises the region of relatively low momenta that dominates the spectrum of hadrons inside a jet. Indeed, the emission of successive gluons inside a jet follows a parton cascade where the emission angles decrease as the jet evolves towards the hadronisation stage, the so-called “angular ordering” [1, 3, 4]. Thus, due to QCD colour coherence and interference of gluon radiation, not the softest partons but those with intermediate energies ( $E_h \propto E_{\text{jet}}^{0.3}$ ) multiply most effectively in QCD cascades [4]. As a result, the energy spectrum of hadrons as a function of  $\xi$  takes a typical “hump-backed plateau” (HBP) shape [4, 5], confirmed by jet measurements at LEP [6] and Tevatron [7] colliders, that can be written to first approximation in a Gaussian form of peak  $\bar{\xi}$  and width  $\sigma$ :

$$D^{\text{ch}}(\ln(1/x), Q) \simeq \exp \left[ -\frac{1}{2\sigma^2}(\xi - \bar{\xi})^2 \right], \quad \bar{\xi} = \ln(1/x_{\text{max}}) \rightarrow \frac{1}{2} \ln \left( \frac{Q}{Q_0} \right), \quad (1)$$

where  $Q_0$  is the collinear cut-off parameter of the perturbative expansion which can be pushed down to the value of  $\Lambda_{\text{QCD}}$  (the so-called “limiting spectrum”). Both the HBP peak and width evolve approximately logarithmically with the energy of the jet: the hadron distribution peaks at  $\bar{\xi} \approx 2$  (5) GeV with a dispersion of  $\sigma \approx 0.7$  (1.4) GeV, for a parton with  $E_{\text{jet}} = 10$  GeV (1 TeV).

The measured fragmentation function (1) corresponds to the sum of contributions from the fragmentation  $D_i^h$  of different primary partons  $i = u, d, \dots, g$ :

$$D^h(\ln(1/x), s) = \sum_i \int_0^1 \frac{dz}{z} C_i(s; z, \alpha_s) D_i^h(x/z, s),$$

and, although one cannot compute from perturbation theory the final parton-to-hadron transition encoded in  $D_i^h$ , the evolution of the “intermediate” functions  $D_a^{bc}$  describing the branching of a parton of type  $a$  into partons of type  $b, c$  can be indeed theoretically predicted. The relevant kinematical variables in the parton splitting process are shown in Fig. 1 for the splitting  $a(k) \rightarrow b(k_1) + c(k_2)$ , such that  $b$  and  $c$  carry the energy-momentum fractions  $z$  and  $(1-z)$  of  $a$  respectively. The Sudakov parametrisation for  $k_1$  and  $k_2$ , the four-momentum of partons  $b$  and  $c$ , can be written as

$$k_1^\mu = zk^\mu - k_\perp^\mu + \frac{\vec{k}^2 + k_\perp^2}{z} \frac{n^\mu}{n \cdot k}, \quad k_2^\mu = (1-z)k^\mu + k_\perp^\mu + \frac{\vec{k}^2 + k_\perp^2}{1-z} \frac{n^\mu}{2n \cdot k}, \quad (2)$$

with the light-like vector  $n^2 = 0$ , and time-like transverse momentum  $k_\perp^2 > 0$  such that,  $k \cdot k_\perp = n \cdot k_\perp = 0$ . Then, the scalar product  $k_1 \cdot k_2$  reads:

$$k_\perp^2 = 2z(1-z)k_1 \cdot k_2. \quad (3)$$

Writing now the 4-momenta  $k = (E, \vec{k})$ ,  $k_1 = (zE, \vec{k}_1)$ ,  $k_2 = ((1-z)E, \vec{k}_2)$  one has,  $|\vec{k}_1| = zE$ ,  $|\vec{k}_2| = (1-z)E$  for on-shell and massless partons  $k_i^2 \approx 0$ . From energy-momentum conservation:

$$k^2 = 2k_1 \cdot k_2 = 2z(1-z)E^2(1 - \cos \theta) \quad (4)$$

such that, replacing Eq. (4) in (3), one finally obtains:

$$k_\perp = 2z(1-z)E \sin \frac{\theta}{2}. \quad (5)$$

In the collinear limit, one is left with  $k_\perp \approx z(1-z)Q$ , where  $Q = E\theta$  is the jet virtuality, or transverse momentum of the jet.

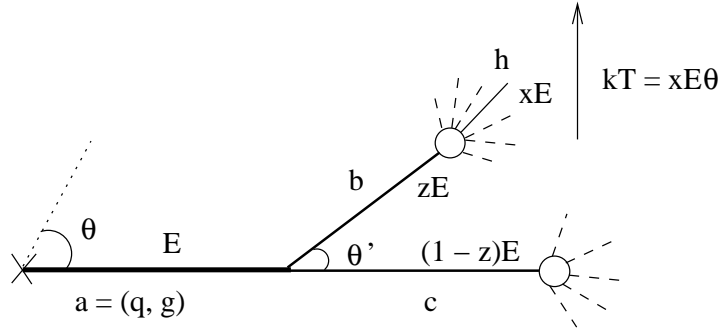


Figure 1: Relevant kinematical variables in the parton splitting process  $a \rightarrow bc$ :  $E$  is the energy of the leading quark or gluon of virtuality  $Q = E\theta$ ;  $z$  and  $(1-z)$  are the energy fractions of the intermediate offsprings  $b$  and  $c$  which finally fragment (at virtualities  $Q_0$ ) into hadrons carrying a fraction  $x$  of the parent parton momentum.

The calculation of the evolution of  $D_a^{bc}$  inside a jet suffers from two types of singularities at each order in the strong coupling  $\alpha_s$ : collinear  $\ln \theta$ -singularities when the gluon emission angle is very small ( $\theta \rightarrow 0$ ), and infrared  $\ln(1/z)$ -singularities when the emitted gluon takes a very small fraction  $z$  of the energy of the parent parton. Various perturbative resummation schemes have been developed to deal with such singularities: (i) the Leading Logarithmic Approximation (LLA) resums single logs of the type  $[\alpha_s \ln(k_\perp^2/\mu^2)]^n$  where  $k_\perp$  is the transverse momentum of the emitted gluon with respect to the parent parton, (ii) the Double Logarithmic Approximation (DLA) resums soft-collinear and infrared gluons,  $g \rightarrow gg$  and  $q(\bar{q}) \rightarrow gq(\bar{q})$ , for small values of  $x$  and  $\theta$   $[\alpha_s \ln(1/z) \ln \theta]^n \sim \mathcal{O}(1)$  [8, 9], (iii) Single Logarithms (SL) [4, 10] account for the emission of hard collinear gluons ( $\theta \rightarrow 0$ ),  $[\alpha_s \ln \theta]^n \sim \mathcal{O}(\sqrt{\alpha_s})$ , and (iv) the Modified Leading Logarithmic Approximation (MLLA) provides a SL correction to the DLA, resumming terms of order  $[\alpha_s \ln(1/z) \ln \theta + \alpha_s \ln \theta]^n \sim [\mathcal{O}(1) + (\mathcal{O}(\sqrt{\alpha_s}))]$  [4]. While the DLA resummation scheme [10] is known to overestimate the cascading process, as it neglects the recoil of the parent parton with respect to its offspring after radiation [9], the MLLA approximation reproduces very well the  $e^+e^-$  data, although Tevatron jet results require further (next-to-MLLA, or NMLLA) refinements [11, 12]. The MLLA [4], partially restores the energy-momentum balance by including SL corrections of order  $\mathcal{O}(\sqrt{\alpha_s})$  coming from the emission of hard-collinear gluons and quarks at large  $x \sim 1$  and small  $\theta_i$  ( $g \rightarrow gg$ ,  $q(\bar{q}) \rightarrow gq(\bar{q})$  and  $g \rightarrow q\bar{q}$ ). Such corrections are included in the standard Dokshitzer-Gribov-Lipatov-Altarelli-Parisi (DGLAP) [13–15] splitting functions which describe the parton evolution at intermediate and large  $x$  in the (time-like) FFs and (space-like) parton distribution functions (PDFs). The first comparison of the MLLA analytical results to the inclusive particle spectra in jets, determining

the energy evolution of the HBP peak position was performed in [16].

The solution of the evolution equations for the gluon and quark jets is usually obtained writing the FF in the form

$$D \simeq C(\alpha_s(t)) \exp \left[ \int^t \gamma(\alpha_s(t')) dt \right], \quad t = \ln Q$$

where  $C(\alpha_s(t)) = 1 + \sqrt{\alpha_s} + \alpha_s \dots$  are the coefficient functions, and  $\gamma = 1 + \sqrt{\alpha_s} + \alpha_s \dots$  is the so-called anomalous dimension, which in Mellin space at LLA reads,

$$\gamma^{\text{LLA}}(\omega, \alpha_s) = \frac{1}{4} \left( -\omega + \sqrt{\omega^2 + 8N_c\alpha_s/\pi} \right).$$

where  $\omega$  is the energy of the radiated gluon and  $N_c$  the number of colours. At small  $\omega$  or  $x$ , the expansion of the FF expression leads to a series of half-powers of  $\alpha_s$ ,  $\gamma \simeq \sqrt{\alpha_s} + \alpha_s + \alpha_s^{3/2} + \dots$ , while at larger  $\omega$  or  $x$  in DGLAP, the expansion yields to a series of integer powers of  $\alpha_s$ ,  $\gamma \simeq \alpha_s + \alpha_s^2 + \alpha_s^3 + \dots$  for FFs and PDFs. In the present work we are mostly concerned with series of half-powers of  $\sqrt{\alpha_s}$  generated at small  $\omega$ , which can be truncated beyond  $\mathcal{O}(\alpha_s)$  in the high-energy limit.

In this paper, the set of next-to-MLLA corrections of order  $\mathcal{O}(\alpha_s)$  for the single inclusive hadron distribution in jets, which further improve energy conservation [17, 18], including in addition the running of the coupling constant  $\alpha_s$  at two-loop or next-to-leading order (NLO) [19], are computed for the first time. Corrections beyond MLLA were considered first in [20], and more recently in [21], for the calculation of the jet mean multiplicity  $\mathcal{N}$  and the ratio  $r = \mathcal{N}_g/\mathcal{N}_q$  in gluon and quark jets. We will follow the resummation scheme presented in [20] and apply it not just to the jet multiplicities but extend it to the full properties of parton fragmentation functions using the distorted Gaussian (DG) parametrisation [22] for the HBP which was only used so far to compute the evolution of FFs at MLLA. The approach followed consists in writing the exponential of Eq. (1) as a DG with mean peak  $\bar{\xi}$  and width  $\sigma$ , including higher moments (skewness and kurtosis) that provide an improved shape of the quasi-Gaussian behaviour of the final distribution of hadrons, and compute the energy evolution of all its (normalised) moments at NMLLA+NLO\* accuracy, which just depend on  $\Lambda_{\text{QCD}}$  as a single free parameter.

Since the evolution of each moment is independent of the ansatz for the initial conditions assumed for the jet hadron spectrum, and since each moment evolves independently of one another, we can obtain five different constraints on  $\Lambda_{\text{QCD}}$ . By fitting all the measured  $e^+e^-$  jet distributions in the range of collision energies  $\sqrt{s} \approx 2\text{--}200$  GeV [6, 23–34, 34–37] a value of  $\Lambda_{\text{QCD}}$  can be extracted which agrees very well with that obtained from the NLO coupling constant evaluated at the  $Z$  resonance,  $\alpha_s(m_Z^2)$ , in the minimal subtraction ( $\overline{\text{MS}}$ ) factorisation scheme [38–40]. Similar studies –at (N)MLLA+LO accuracy under different approximations, and with a more reduced experimental data-set– were done previously for various parametrizations of the input fragmentation function [41–44] but only with a relatively modest data-theory agreement, and an extracted LO value of  $\Lambda_{\text{QCD}}$  with large uncertainties.

The paper is organised as follows. In Sect. 2 we write the evolution equations and provide the generic solution including the set of  $\mathcal{O}(\alpha_s)$  terms from the splitting functions in Mellin space. In subsection 3.1, the new NMLLA+NLO\* anomalous dimension,  $\gamma_\omega^{\text{NMLLA+NLO*}}$ , is obtained from the evolution equations in Mellin space, being the main theoretical result of this paper. In subsection 3.2 the Fong and Webber DG parametrisation [22] for the single-inclusive hadron distribution is used and the energy evolution of its moments (mean multiplicity, peak position, width, skewness and kurtosis) is computed making use of  $\gamma_\omega^{\text{NMLLA+NLO*}}$ . In subsection 3.3, the results of our approach are compared for the quark and gluon

multiplicities, recovering the NMLLA multiplicity ratio first obtained in [17]. The energy-evolution for all the moments in the limiting spectrum case ( $Q_0 \rightarrow \Lambda_{\text{QCD}}$ ) are derived in subsection 3.4, and the role of higher-order corrections contributing to the resummed components of the DG which improve the overall behaviour of the perturbative series, are discussed in subsection 3.5, and the final analytical formulæ are provided. Subsection 3.6 discusses our treatment of finite-mass effects and heavy-quark thresholds, as well as other subleading corrections. The phenomenological comparison of our analytical results to the world  $e^+e^-$  jet data is carried out in Sect. 4, from which a value of  $\Lambda_{\text{QCD}}$  can be extracted from the fits. Our results are summarised in Sect. 5 and the appendices provide more details on various ingredients used in the calculations.

## 2 Evolution equations for the low- $x$ parton fragmentation functions

The fragmentation function of a parton  $a$  splitting into partons  $b$  and  $c$  satisfies the following system of evolution equations [4, 5] as a function of the variables defined in Fig. 1:

$$\frac{\partial}{\partial \ln \theta} x D_a^b(x, \ln E\theta) = \sum_c \int_0^1 dz \frac{\alpha_s(k_\perp^2)}{2\pi} P_{ac}(z) \left[ \frac{x}{z} D_c^b\left(\frac{x}{z}, \ln z E\theta\right) \right], \quad (6)$$

where  $P_{ac}(z)$  are the regularised DGLAP splitting functions [13–15], which at LO are given by

$$P_{qg}(z) = 4C_F \left( \frac{1}{z} + \frac{z}{2} - 1 \right), \quad P_{qq}(z) = 2C_F \left( \left[ \frac{1}{1-z} \right]_+ - \frac{z}{2} - \frac{1}{2} \right), \quad (7)$$

$$P_{gg}(z) = 2C_A \left( \frac{1}{z} + \left[ \frac{1}{1-z} \right]_+ + z(1-z) - 2 \right), \quad P_{gq}(z) = n_f T_R [z^2 + (1-z)^2], \quad (8)$$

with  $C_F = (N_c^2 - 1)/2N_c$  and  $N_c$  respectively the Casimirs of the fundamental and adjoint representation of the QCD colour group  $SU(3)_c$ ,  $T_R = 1/2$ , and  $n_f$  is the number of active (anti)quark flavours. The regularisation of the splitting functions in Eq. (6) is performed through the  $+$  distribution<sup>‡</sup> in Eqs. (7) and (8). The  $\alpha_s$  is the strong coupling which at the two-loop level reads [19]

$$\alpha_s(q^2) = \frac{4\pi}{\beta_0 \ln q^2} \left[ 1 - \frac{2\beta_1}{\beta_0^2} \frac{\ln \ln q^2}{\ln q^2} \right], \quad \text{for } q^2 = \frac{k_\perp^2}{\Lambda_{\text{QCD}}^2}, \quad (9)$$

with

$$\beta_0 = \frac{11}{3}N_c - \frac{4n_f T_R}{3}, \quad \beta_1 = \frac{51}{3}N_c - \frac{38n_f T_R}{3},$$

being the first two coefficients involved in the perturbative expansion of the  $\beta$ -function through the renormalisation group equation:

$$\beta(\alpha_s) = -\beta_0 \frac{\alpha_s^2}{2\pi} - \beta_1 \frac{\alpha_s^3}{4\pi^2} + \mathcal{O}(\alpha_s^4).$$

The initial condition for the system of evolution equations (6) is given by a delta function

$$x D_a^b(x, \ln E\theta) \big|_{(\ln E\theta = \ln Q_0)} = \delta_a^b \cdot \delta(1-x)$$

running “backwards” from the end of the parton branching process, with a clear physical interpretation: when the transverse momentum of the leading parton is low enough, it can not fragment ( $x = 1$ ) and

---

<sup>‡</sup>The plus distribution applied to a function  $F(x)$ , written  $[F(x)]_+$ , is defined as  $\int_0^1 dx [F(x)]_+ g(x) = \int_0^1 dx [F(x)] (g(x) - g(1))$  for any function  $g(x)$ .

hadronises into a single hadron. The equations (6) are identical to the DGLAP evolution equations but for one detail, the shift in  $\ln z$  in the second argument of the fragmentation function  $\frac{x}{z} D_c^b\left(\frac{x}{z}, \ln z + \ln E\theta\right)$ , that for hard partons is set to zero,  $\ln z \sim 0$ , in the LLA. It corresponds to the so-called scaling violation of DGLAP FFs in time-like evolution, and that of space-like evolution of PDFs in DIS. In our framework, however, this term is responsible for the double soft-collinear contributions that are resummed at all orders as  $(\alpha_s \ln^2)^n$ , justifying the fact that the approach is said to be modified (MLLA) with respect to the LLA.

The evolution equations are commonly expressed as a function of two variables:

$$Y = \ln \frac{E\theta}{Q_0}, \quad \lambda = \ln \frac{Q_0}{\Lambda_{\text{QCD}}}, \quad (10)$$

where  $Y$  provides the parton-energy dependence of the fragmentation process, and the  $\lambda$  specifies, in units of  $\Lambda_{\text{QCD}}$ , the value of the hadronisation scale  $Q_0$  down to which the parton shower is evolved. Standard parton showers Monte Carlo codes, such as PYTHIA [45], use  $Q_0$  values of the order of  $\mathcal{O}(1 \text{ GeV})$  whereas in the limiting spectrum [4], that will be used here, it can be taken as low as  $\lambda \rightarrow 0$ , i.e.  $Q_0 \rightarrow \Lambda_{\text{QCD}}$ . Applying the Mellin transform to the single inclusive distribution in Eq. (6)

$$\mathcal{D}(\omega, Y) = \int_0^\infty d\xi e^{-\omega\xi} D(\xi, Y), \quad (11)$$

and introducing

$$\hat{\xi} = \ln \frac{1}{z}, \quad \hat{y} = \ln \frac{k_\perp}{Q_0}, \quad \hat{\xi} + \hat{y} = \ln \frac{E\theta}{Q_0} \equiv Y, \quad (12)$$

with  $k_\perp \approx zE\theta$  in the soft approximation ( $z \ll 1$ ), one is left with the integro-differential system of evolution equations for the non-singlet distributions

$$\frac{\partial}{\partial Y} \mathcal{D}(\omega, Y) = \int_0^\infty d\hat{\xi} e^{-\omega\hat{\xi}} P(\hat{\xi}) \frac{\alpha_s(Y - \hat{\xi})}{2\pi} \mathcal{D}(\omega, Y - \hat{\xi}), \quad (13)$$

where

$$P(\hat{\xi}) = \begin{pmatrix} P_{qq}(\hat{\xi}) & P_{qg}(\hat{\xi}) \\ P_{gq}(\hat{\xi}) & P_{gg}(\hat{\xi}) \end{pmatrix}, \quad \mathcal{D}(\omega, \hat{y}) = \begin{pmatrix} \mathcal{D}_q(\omega, \hat{y}) \\ \mathcal{D}_g(\omega, \hat{y}) \end{pmatrix} \quad (14)$$

and the lower and upper indices have been omitted for the sake of simplicity. The NLO strong coupling (9) can be rewritten as a function of the new variables (12), such that

$$\alpha_s(\hat{y}) = \frac{2\pi}{\beta_0(\hat{y} + \lambda)} \left[ 1 - \frac{\beta_1}{\beta_0^2} \frac{\ln 2(\hat{y} + \lambda)}{\hat{y} + \lambda} \right], \quad \hat{y} = Y - \hat{\xi}. \quad (15)$$

The parton density  $x D(x, Y)$  is then obtained through the inverse Mellin transform:

$$D(\hat{\xi}, Y) = \int_C \frac{d\omega}{2\pi i} e^{\omega\hat{\xi}} \mathcal{D}(\omega, Y) \quad (16)$$

where the contour  $C$  lies to the right of all singularities in the  $\omega$ -complex plane. In the high-energy limit ( $Q \gg Q_0$ ) and hard fragmentation region ( $Y \gg \hat{\xi}$  or  $x \sim 1$ ), one can replace in the r.h.s. of Eq. (13) the following expansion<sup>§</sup>:

$$\alpha_s(Y - \bar{\xi}) \mathcal{D}(\omega, Y - \bar{\xi}) = e^{-\bar{\xi} \frac{\partial}{\partial Y}} \alpha_s(Y) \mathcal{D}(\omega, Y), \quad e^{-\bar{\xi} \frac{\partial}{\partial Y}} = \sum_{n=0}^{\infty} \frac{(-1)^n}{n!} \frac{\partial^n}{\partial Y^n}. \quad (17)$$

---

<sup>§</sup>Note that the MLLA solution [4] to the evolution equations corresponds to the replacement  $\alpha_s(Y - \bar{\xi}) \mathcal{D}(\omega, Y - \bar{\xi}) \approx \alpha_s(Y) \mathcal{D}(\omega, Y)$  accounting for the single logarithmic corrections of relative order  $\mathcal{O}(\sqrt{\alpha_s})$ .

Thus, replacing Eq. (17) into (13) one obtains

$$\frac{\partial}{\partial Y} \mathcal{D}(\omega, Y) = \left( \int_0^\infty d\hat{\xi} e^{-\Omega \hat{\xi}} P(\hat{\xi}) \right) \frac{\alpha_s(Y)}{2\pi} \mathcal{D}(\omega, Y), \quad (18)$$

which allows for the factorisation of  $\alpha_s(Y) \mathcal{D}(\omega, Y)$ , and leads to the equation

$$\frac{\partial}{\partial Y} \mathcal{D}(\omega, Y) = P(\Omega) \frac{\alpha_s(Y)}{2\pi} \mathcal{D}(\omega, Y), \quad P(\Omega) = \int_0^\infty d\hat{\xi} e^{-\Omega \hat{\xi}} P(\hat{\xi}), \quad (19)$$

more suitable for analytical solutions. Truncating the series at higher orders translates into including corrections  $\mathcal{O}(\alpha_s)$  which better account for energy conservation, particularly at large  $x$ . In Mellin space, the expansion can be made in terms of the differential operator  $\Omega \equiv \omega + \partial/\partial Y$  such that, up to the second term in  $\Omega$ , one is left with NMLLA corrections of order  $\mathcal{O}(\alpha_s)$  [11]. Explicitly, the inclusion of higher-order corrections from the second term of  $\alpha_s(Y - \bar{\xi}) \mathcal{D}(\omega, Y - \bar{\xi}) \approx \alpha_s \mathcal{D} - \bar{\xi} \partial(\alpha_s \mathcal{D})/\partial Y$ , followed by the integration over the splitting functions (7)–(8) in  $x$  space in the r.h.s. of Eq. (13), is equivalent to the expansion  $P(\Omega) = P^{(0)} + P^{(1)}\Omega$  in Mellin space in the r.h.s. of (19), where  $P^{(0)}$  and  $P^{(1)}$  are constants. The expansion of the matrix elements  $P(\Omega)$  in  $\Omega$  can be obtained from the original expressions of the Mellin transformed splitting functions [46], as given in Eqs. (114a)–(114d) in Appendix A, which leads to the following expressions:

$$P_{gg}(\Omega) = \frac{4N_c}{\Omega} - \frac{11}{3}N_c - \frac{4}{3}n_f T_R + 4N_c \left( \frac{67}{36} - \frac{\pi^2}{6} \right) \Omega + \mathcal{O}(\Omega^2), \quad (20a)$$

$$P_{gq}(\Omega) = \frac{8n_f T_R}{3} - \frac{26n_f T_R}{9} \Omega + \mathcal{O}(\Omega^2), \quad (20b)$$

$$P_{qg}(\Omega) = \frac{4C_F}{\Omega} - 3C_F + \frac{7}{2}C_F \Omega + \mathcal{O}(\Omega^2), \quad (20c)$$

$$P_{qq}(\Omega) = 4C_F \left( \frac{5}{8} - \frac{\pi^2}{6} \right) \Omega + \mathcal{O}(\Omega^2). \quad (20d)$$

where the finite terms for  $\Omega \rightarrow 0$  constitute the new subset to be computed for the first time in this work. The solution of the evolution equations in the MLLA were considered in [4] up to the regular terms with  $\delta P_{qq}(\Omega)\Omega = 0$ . By including those proportional to  $\Omega$ , one is in addition considering the set of higher-order corrections  $\mathcal{O}(\alpha_s)$  known as NMLLA that improve energy conservation [20]. The diagonalisation of the matrix (14) in order to solve (19) results into two trajectories (eigenvalues), which can be written as [4, 46]

$$P_{\pm\pm}(\Omega) = \frac{1}{2} \left[ P_{gg}(\Omega) + P_{qq}(\Omega) \pm \sqrt{(P_{gg}(\Omega) - P_{qq}(\Omega))^2 + 4P_{gq}(\Omega)P_{qg}(\Omega)} \right]. \quad (21)$$

Substituting Eqs. (20a)–(20d) into (21) and performing the expansion again up to terms  $\mathcal{O}(\Omega)$ , yields:

$$P_{++}(\Omega) = \frac{4N_c}{\Omega} - a_1 + 4N_c a_2 \Omega + \mathcal{O}(\Omega^2), \quad (22a)$$

$$P_{--}(\Omega) = -b_1 + 4C_F b_2 \Omega + \mathcal{O}(\Omega^2), \quad (22b)$$

where the terms proportional to  $\Omega$  are new in this framework. The set of constants involved in Eqs. (22a)

and (22b) reads:

$$a_1 = \frac{11}{3}N_c + \frac{4}{3}n_f T_R \left(1 - 2\frac{C_F}{N_c}\right), \quad (23a)$$

$$a_2 = \frac{67}{36} - \frac{\pi^2}{6} - \frac{n_f T_R C_F}{18N_c^2} \left[ \frac{11}{3}N_c - 4\frac{n_f T_R}{N_c} \left(1 - 2\frac{C_F}{N_c}\right) \right], \quad (23b)$$

$$b_1 = \frac{8n_f T_R C_F}{3N_c}, \quad (23c)$$

$$b_2 = \frac{5}{8} - \frac{\pi^2}{6} + \frac{n_f T_R}{18N_c} \left[ \frac{11}{3}N_c - 4\frac{n_f T_R}{N_c} \left(1 - 2\frac{C_F}{N_c}\right) \right]. \quad (23d)$$

Therefore, the diagonalisation of Eq. (19) leads to two equations:

$$\frac{\partial}{\partial Y} \mathcal{D}^\pm(\omega, Y, \lambda) = P_{\pm\pm}(\Omega) \frac{\alpha_s(Y)}{2\pi} \mathcal{D}^\pm(\omega, Y, \lambda), \quad (24)$$

such that in the new  $\mathcal{D}^\pm$ -basis the respective solutions read:

$$\mathcal{D}_q(\omega, Y, \lambda) = \frac{P_{qg}(\Omega)}{P_{++}(\Omega) - P_{--}(\Omega)} [\mathcal{D}^+(\omega, Y, \lambda) - \mathcal{D}^-(\omega, Y, \lambda)], \quad (25a)$$

$$\mathcal{D}_g(\omega, Y, \lambda) = \frac{P_{++}(\Omega) - P_{qq}(\Omega)}{P_{++}(\Omega) - P_{--}(\Omega)} \mathcal{D}^+(\omega, Y, \lambda) - \frac{P_{--}(\Omega) - P_{qg}(\Omega)}{P_{++}(\Omega) - P_{--}(\Omega)} \mathcal{D}^-(\omega, Y, \lambda). \quad (25b)$$

where the ratios in front of  $\mathcal{D}^\pm$  are the coefficient functions that will be evaluated hereafter. Notice that in the  $\mathcal{D}^\pm$  basis, the off-diagonal terms  $P_{+-}(\Omega) = 0$  and  $P_{-+}(\Omega) = 0$  vanish for LO splitting functions, while this is no longer true for time-like splitting functions obtained from the  $\overline{\text{MS}}$  factorisation scheme beyond LO [47], as explained in [21] for multiparticle production. Following this logic,  $\mathcal{D}^\pm$  should first be determined in order to obtain the gluon and quark jets single inclusive distributions.

### 3 Evolution of the parton fragmentation functions at NMLLA +NLO\*

#### 3.1 Anomalous dimension at NMLLA +NLO\*

Our NMLLA+NLO\* scheme involves adding further corrections  $\mathcal{O}(\alpha_s)$  from contributions proportional to  $\Omega$  in the Mellin representation of the expanded splitting functions, and considering the two-loop strong coupling, Eq. (15). We label our approach as NLO\* to indicate that the full set of NLO corrections are only approximately included, as the two-loop splitting functions (discussed e.g. in [21]) are not incorporated. After diagonalisation of the original evolution equations (6), the Eqs. (24) for  $\mathcal{D}^\pm$  result in the following expressions for  $\mathcal{D}^+$  and  $\mathcal{D}^-$ :

$$\left(\omega + \frac{\partial}{\partial Y}\right) \frac{\partial}{\partial Y} \mathcal{D}^+(\omega, Y, \lambda) = \left[1 - \frac{a_1}{4N_c} \left(\omega + \frac{\partial}{\partial Y}\right) + a_2 \left(\omega + \frac{\partial}{\partial Y}\right)^2\right] 4N_c \frac{\alpha_s}{2\pi} \mathcal{D}^+(\omega, Y, \lambda) \quad (26)$$

$$\frac{\partial}{\partial Y} \mathcal{D}^-(\omega, Y, \lambda) = -b_1 \frac{\alpha_s}{2\pi} \mathcal{D}^-(\omega, Y, \lambda) + 4C_F b_2 \left(\omega + \frac{\partial}{\partial Y}\right) \frac{\alpha_s}{2\pi} \mathcal{D}^-(\omega, Y, \lambda). \quad (27)$$

The leading contribution to  $\mathcal{D}^-$  after setting  $b_2 = 0$  in Eq. (27) reads:

$$\mathcal{D}^-(\omega, Y, \lambda) \approx \left(\frac{\lambda}{Y + \lambda}\right)^{\frac{b_1}{4N_c\beta_0}} \mathcal{D}^-(\omega, \lambda). \quad (28)$$



The exponent  $b_1/(4N_c\beta_0) = \mathcal{O}(10^{-2}\sqrt{\alpha_s})$  induces a very small (non-Gaussian) correction, which can be neglected asymptotically, for  $Y + \lambda \gg \lambda$ . Thus, the (+) trajectory (22a) provides the main contribution to the single inclusive distribution  $D(\xi, Y) = xD(x, Y)$  at small  $x \ll 1$ , after applying the inverse Mellin transform (16). Hard corrections proportional to  $a_1$  and  $a_2$  account for the energy balance in the hard fragmentation region and are of relative order  $\mathcal{O}(\sqrt{\alpha_s})$  and  $\mathcal{O}(\alpha_s)$  respectively with respect to the  $\mathcal{O}(1)$  DLA contribution. The NLO expression (9) results in corrections  $\propto \beta_0$  at MLLA, and  $\propto \beta_0, \beta_1$  at NMLLA which provide a more accurate consideration of running coupling effects at small  $x \ll 1$  [20]. In Ref. [20], the mean multiplicities, multiplicity correlators in gluon and quark jets, and the ratio of gluon and quark jet multiplicities were also studied at NMLLA, where corrections  $\propto \beta_1$  were accordingly included. Here, we extend the NMLLA analysis to all moments of the fragmentation function.

The solution of Eq. (26) can be written in the compact form:

$$\mathcal{D}^+(\omega, Y, \lambda) = E_+(\omega, \alpha_s(Y + \lambda))\mathcal{D}^+(\omega, \lambda), \quad (29)$$

with the evolution “Hamiltonian”:

$$E_+(\omega, \alpha_s(Y + \lambda)) = \exp \left[ \int_0^Y dy \gamma(\omega, \alpha_s(y + \lambda)) \right]. \quad (30)$$

that describes the parton jet evolution from its initial virtuality  $Q$  to the lowest possible energy scale  $Q_0$ , at which the parton-to-hadron transition occurs. In Eq. (30),  $\gamma(\omega, \alpha_s(y))$  is the anomalous dimension that mixes  $g \rightarrow gg$  and  $g \rightarrow q\bar{q}$  splittings and is mainly dominated by soft gluon bremsstrahlung ( $g \rightarrow gg$ ). Introducing the shorthand notation  $\gamma_\omega = \gamma(\omega, \alpha_s(Y))$ , the MLLA anomalous dimension has been determined in the past [4, 22], setting  $a_2 = 0$  and  $\beta_1 = 0$  in Eq. (26), and is given by

$$\begin{aligned} \gamma_\omega^{\text{MLLA}} = & \frac{1}{2} \left( -\omega + \sqrt{\omega^2 + 4\gamma_0^2} \right) \\ & + \frac{\alpha_s}{2\pi} \left[ -\frac{1}{2}a_1 \left( 1 + \frac{\omega}{\sqrt{\omega^2 + 4\gamma_0^2}} \right) + \beta_0 \frac{\gamma_0^2}{\omega^2 + 4\gamma_0^2} \right] + \mathcal{O}(\alpha_s^{3/2}), \end{aligned} \quad (31)$$

where  $\gamma_0^2$  is the DLA anomalous dimension amounting to

$$\gamma_0^2 = \frac{4N_c\alpha_s}{2\pi} = \frac{4N_c}{\beta_0(Y + \lambda)}. \quad (32)$$

The first term of Eq. (31) is the DLA main contribution, of order  $\mathcal{O}(\sqrt{\alpha_s})$ , which physically accounts for soft gluon multiplication, the second and third terms are SL corrections  $\mathcal{O}(\alpha_s)$  accounting for the energy balance ( $\propto a_1$ ) and running coupling effects ( $\propto \beta_0$ ). It is important to make the difference between orders and relative orders mentioned above. Indeed, if one looks at the l.h.s. of the evolution equation (26) for  $\mathcal{D}^+$ ,  $(\omega + \partial/\partial Y)\partial\mathcal{D}^+/\partial Y = \mathcal{O}(\alpha_s)$ , the first term in the r.h.s. is  $\mathcal{O}(\alpha_s)$ , the second one proportional to  $a_1$  is  $\mathcal{O}(\alpha_s^{3/2})$ , and the third one, proportional to  $a_2$ , is  $\mathcal{O}(\alpha_s^2)$  such that after factorising the whole equation by  $\mathcal{O}(\alpha_s)$  one is left with the relative orders of magnitude in  $\sqrt{\alpha_s}$ . Setting Eq. (29) in (26) leads to the perturbative differential equation

$$(\omega + \gamma_\omega)\gamma_\omega - \frac{2N_c\alpha_s}{\pi} = -\beta(\alpha_s)\frac{d\gamma_\omega}{d\alpha_s} - a_1(\omega + \gamma_\omega)\frac{\alpha_s}{2\pi} - \frac{a_1}{2\pi}\beta(\alpha_s) + a_2(\omega^2 + 2\omega\gamma_\omega + \gamma_\omega^2)\frac{\alpha_s}{2\pi}, \quad (33)$$

which will be solved after inserting the two-loop coupling (9) in order to include corrections  $\propto \beta_1$  as well. The equation can be solved iteratively (perturbatively) by setting the MLLA anomalous dimension

written in Eq. (31) in the main and subleading contributions of Eq. (33), to find:

$$\begin{aligned}\gamma_\omega^{\text{NMLLA+NLO}^*} &= \gamma_\omega^{\text{MLLA}} + \frac{\gamma_0^4}{16N_c^2} \left\{ a_1^2 \frac{\gamma_0^2}{(\omega^2 + 4\gamma_0^2)^{3/2}} + \frac{a_1\beta_0}{2} \left( \frac{1}{\sqrt{\omega^2 + 4\gamma_0^2}} - \frac{\omega^3}{(\omega^2 + 4\gamma_0^2)^2} \right) \right. \\ &\quad \left. + \beta_0^2 \left( \frac{2\gamma_0^2}{(\omega^2 + 4\gamma_0^2)^{3/2}} - \frac{5\gamma_0^4}{(\omega^2 + 4\gamma_0^2)^{5/2}} \right) - 4N_c \frac{\beta_1 \ln 2(Y + \lambda)}{\beta_0 \sqrt{\omega^2 + 4\gamma_0^2}} \right\} \\ &\quad + \frac{1}{4} a_2 \gamma_0^2 \left[ \frac{\omega}{(\omega^2 + 4\gamma_0^2)^{1/4}} + (\omega^2 + 4\gamma_0^2)^{1/4} \right]^2 + \mathcal{O}(\gamma_0^4),\end{aligned}\tag{34}$$

which is the main theoretical result of this paper. Terms proportional to  $a_1^2$ ,  $a_1\beta_0$  and  $\beta_0^2$  are of order  $\mathcal{O}(\alpha_s^{3/2})$ , and were previously calculated in the (N)MLLA+LO scheme described in [42]. Those proportional to  $\beta_1$  and  $a_2$  are computed for the first time in our NMLLA+NLO\* framework. Indeed, the single correction  $\propto \beta_1$  is obtained replacing Eq. (9) in the l.h.s. of (33), which leads to the equation,

$$\gamma_\omega^2 + \omega\gamma_\omega - \gamma_0^2 + \frac{\beta_1}{4N_c\beta_0} \gamma_0^4 \ln 2(Y + \lambda) + \dots = 0 \Rightarrow \gamma_\omega = \gamma_\omega^{\text{DLA}} - \frac{\gamma_0^4}{4N_c} \left\{ \frac{\beta_1 \ln 2(Y + \lambda)}{\beta_0 \sqrt{\omega^2 + 4\gamma_0^2}} + \dots \right\}$$

with  $\gamma_\omega^{\text{DLA}} = \frac{1}{2} \left( -\omega + \sqrt{\omega^2 + 4\gamma_0^2} \right)$ . Since  $\ln(Y + \lambda) = \mathcal{O}(1)$  and  $\omega = \mathcal{O}(\sqrt{\alpha_s})$ , and following  $\alpha_s$  power counting, this correction has naturally the same order of magnitude  $\mathcal{O}(\alpha_s^{3/2})$  as the other terms and should not be neglected. The other new correction  $\propto a_2\gamma_0^2 \propto \alpha_s$  adds those NMLLA contributions arising from the  $\propto \omega$  terms in the LO splitting functions (20a)–(20d), known to better account for energy conservation. Since this correction is multiplied by a term  $[\dots]^2 = \mathcal{O}(\sqrt{\alpha_s})$ , the overall result is  $\mathcal{O}(\alpha_s^{3/2})$  and, thus, of the same order of magnitude as the previous terms such that, the full resummed result is  $\mathcal{O}(\alpha_s^{3/2})$ .

### 3.2 Distorted Gaussian (DG) parametrisation for the fragmentation function

The distorted Gaussian (DG) parametrisation of the single inclusive distribution of hadrons in jets at small  $x$  (or  $\omega \rightarrow 0$ ) was introduced by Fong and Webber in 1991 [22], and in  $x$ -space it reads:

$$D^+(\xi, Y, \lambda) = \frac{\mathcal{N}}{\sigma\sqrt{2\pi}} \exp \left[ \frac{1}{8}k - \frac{1}{2}s\delta - \frac{1}{4}(2+k)\delta^2 + \frac{1}{6}s\delta^3 + \frac{1}{24}k\delta^4 \right],\tag{35}$$

where,  $\delta = (\xi - \bar{\xi})/\sigma$ ,  $\mathcal{N}$  is the asymptotic average multiplicity inside a jet, and  $\bar{\xi}$ ,  $\sigma$ ,  $s$ , and  $k$  are respectively the mean peak position, the dispersion, the skewness, and kurtosis of the distribution. The distribution should be displayed in the interval  $0 \leq \xi \leq Y$  which depends on the jet energy, and the values of  $Q_0$  and  $\Lambda_{\text{QCD}}$ . The three scales of the process are organised in the form  $Q \gg Q_0 \geq \Lambda_{\text{QCD}}$ . The formula (35) reduces to a Gaussian for  $s = k = 0$  and its generic expression does not depend on the approach or level of accuracy used for the computation of its evolution.

As an example of the effects of non-zero skewness and kurtosis, we compare in Fig. 2 the shapes of four different single-inclusive hadron distributions of width  $\sigma = 1.4$  and mean position at  $\bar{\xi} = 3.5$  in the interval  $0 \leq \xi \lesssim 7$  typical of jets at LEP-1 energies: (i) an exact Gaussian, (ii) a skewed Gaussian with  $s = -0.5$ ,  $k = 0$ , (iii) a kurtic Gaussian with  $s = 0$ ,  $k = -0.5$ , and (iv) a DG including both “distorting”  $s, k$  components above. As can be seen, the shape of the DG differs from that of the pure Gaussian, mainly away from the hump region. A negative skewness displaces the peak of the Gaussian to higher  $\xi$  values while adding a longer tail to low  $\xi$ , and a negative kurtosis tends to make “fatter” its width.

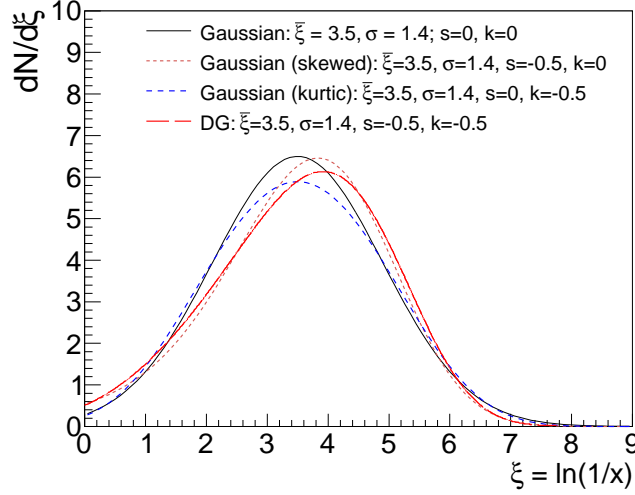


Figure 2: Comparison of various Gaussian-like hadron distributions in jets sharing the same mean  $\xi$  position and width ( $\bar{\xi} = 3.5$  and  $\sigma = 1.4$ ) but with different third and fourth moments: (i) symmetric Gaussian, (ii) skewness  $s = -0.5$ , (iii) negative kurtosis  $k = -0.5$ , and (iv) full distorted Gaussian with  $s = k = -0.5$ .

In order to obtain the evolution of the different DG components, we will proceed by following the same steps as in [22] but making use instead of the expanded NMLLA+NLO\* anomalous dimension, Eq. (34), computed here. Defining  $K_n$  as the  $n$ -th moment of the single inclusive distribution:

$$K_n(Y, \lambda) = \left( -\frac{d}{d\omega} \right)^n \ln [\mathcal{D}^+(\omega, Y, \lambda)]_{\omega=0}, \quad (36)$$

the different components (normalised moments) of the DG are given by<sup>¶</sup>:

$$\mathcal{N} = K_0, \quad \bar{\xi} = K_1, \quad \sigma = \sqrt{K_2}, \quad s = \frac{K_3}{\sigma^3}, \quad k = \frac{K_4}{\sigma^4}, \quad k_5 = \frac{K_5}{\sigma^5}; \quad (37)$$

such that after plugging Eq. (30) into (29) and what results from it into (36), one is left with

$$K_{n \geq 0} = \int_0^Y dy \left( -\frac{\partial}{\partial \omega} \right)^n \gamma_\omega(\alpha_s(y + \lambda)) \Big|_{\omega=0}, \quad (38)$$

which is more suitable for analytical calculations since it directly involves the anomalous dimension expression (34).

**Multiplicity.** The multiplicity is obtained from the zeroth moment, i.e. the integral, of the single-particle distribution. Setting  $\omega = 0$  in Eq. (34), one obtains

$$\begin{aligned} \gamma_\omega(0, \alpha_s) &= \gamma_0 - \frac{1}{8N_c} \left( a_1 - \frac{\beta_0}{2} \right) \gamma_0^2 \\ &+ \frac{1}{2} \left[ a_2 + \frac{1}{32N_c^2} \left( \frac{a_1^2}{2} + a_1\beta_0 + \frac{3\beta_0^2}{8} \right) - \frac{\beta_1 \ln 2(Y + \lambda)}{4N_c\beta_0} \right] \gamma_0^3, \end{aligned} \quad (39)$$

<sup>¶</sup>We list also  $k_5$  which is needed to obtain the maximum peak position  $\xi_{\max}$  from  $\bar{\xi}$ , as discussed below.

from which the mean multiplicity  $\mathcal{N}(Y, \lambda)$  can be straightforwardly derived by integrating over  $y$ :

$$\mathcal{N}(Y, \lambda) = \mathcal{N}_0 \exp [f_{\mathcal{N}}(Y, \lambda) - f_{\mathcal{N}}(0, \lambda)] \quad (40)$$

where

$$\begin{aligned} f_{\mathcal{N}}(y, \lambda) = & \sqrt{\frac{16N_c}{\beta_0}(y + \lambda)} - \left(\frac{a_1}{\beta_0} - \frac{1}{2}\right) \ln \sqrt{(y + \lambda)} - \frac{2N_c}{\beta_0} \left[ a_2 + \frac{1}{4} \left(\frac{a_1}{4N_c}\right)^2 + \frac{a_1\beta_0}{32N_c^2} \right. \\ & \left. + \frac{3}{16} \left(\frac{\beta_0}{4N_c}\right)^2 - \frac{\beta_1}{4N_c\beta_0} (\ln 2(y + \lambda) + 2) \right] \sqrt{\frac{16N_c}{\beta_0(y + \lambda)}}. \end{aligned} \quad (41)$$

As expected, the mean multiplicity (40) including the two-loop  $\alpha_s$  exactly coincides with the expression obtained in [20]. This cross-check supports the validity of our “master” NMLLA+NLO\* formula (34) for the anomalous dimension at small  $\omega$ , which is not surprising as the gluon jet evolution equation solved in [20] for the mean multiplicity coincides with Eq. (26) after setting  $\omega = 0$  and  $\mathcal{N}(Y, \lambda) = \mathcal{D}^+(0, Y, \lambda)$ . The first term in Eq. (41) is the DLA rate of multiparticle production, the second and third terms provide negative corrections that account for energy conservation and decrease the multiplicity. However, the third term, proportional to  $\beta_1$ , is positive and can be large since it accounts for NLO coupling corrections. Though, due to energy conservation, one may expect the multiplicity to decrease in the present scheme running coupling effects take over and can drastically increase the multiplicity as well as single inclusive cross-sections at the energy scales probed so far at  $e^+e^-$  colliders. Only at asymptotically high-energy scales, that is for  $Q_0 \gg \Lambda_{\text{QCD}}$ , the energy conservation becomes dominant over running coupling effects, thus inverting these trends. The ratio of multiplicities in quark and gluon jets are discussed in Sect. 3.3 and compared with the calculations of [20]. Performing the numerical evaluation for  $n_f = 5$  quark flavours<sup>||</sup> we obtain the final expression for the multiplicity:

$$\begin{aligned} \mathcal{N}(Y) \propto \exp & \left[ 2.50217 \left( \sqrt{Y + \lambda} - \sqrt{\lambda} \right) - 0.491546 \ln \frac{Y + \lambda}{\lambda} \right. \\ & \left. - (0.06889 - 0.41151 \ln(Y + \lambda)) \frac{1}{\sqrt{Y + \lambda}} + (0.06889 - 0.41151 \ln \lambda) \frac{1}{\sqrt{\lambda}} \right]. \end{aligned} \quad (42)$$

**Peak position.** The energy evolution dependence of the mean peak position is obtained plugging Eq. (34) into (30), and the latter into Eq. (29) in order to get the  $K_n$  moments of the distribution from Eq. (36). Thus, for  $n = 1$  one obtains

$$\bar{\xi} = \frac{Y}{2} + \frac{a_1}{\sqrt{16N_c\beta_0}} \left( \sqrt{Y + \lambda} - \sqrt{\lambda} \right) - 2N_c \frac{a_2}{\beta_0} (\ln(Y + \lambda) - \ln \lambda), \quad (43)$$

The smallness of the constant in front of the NMLLA correction proportional to  $(\ln(Y + \lambda) - \ln \lambda)$  should not drastically modify the MLLA peak position and should only affect it at small energy scales.

The position of the mean peak is related to the corresponding maximum and median values of the DG distribution by the expressions [48]:

$$\xi_{\text{max}} - \bar{\xi} = -\frac{1}{2}\sigma_s \left( 1 - \frac{1}{4} \frac{k_5}{s} + \frac{5}{6}k \right), \quad \xi_{\text{m}} - \bar{\xi} = -\frac{1}{6}\sigma_s \left( 1 - \frac{3}{20} \frac{k_5}{s} + \frac{1}{2}k \right), \quad (44)$$

---

<sup>||</sup>As will be seen below the dependence in  $n_f$  is very weak and will not affect the final normalisation of the distribution.

for which we need the fifth moment of the DG,  $k_5$ , which reads:

$$k_5(Y, \lambda) = \frac{9}{16} a_1 \left( \frac{3}{Y + \lambda} \right)^{3/2} \left[ \frac{\beta_0(Y + \lambda)}{16N_c} \right]^{1/4} \frac{1 - \left( \frac{\lambda}{Y + \lambda} \right)^{5/2}}{\left[ 1 - \left( \frac{\lambda}{Y + \lambda} \right)^{3/2} \right]^{5/2}} \left[ 1 + 5 \left( \frac{f_1(Y, \lambda)}{64} + \frac{f_4(Y, \lambda)}{72} \right) \beta_0 \sqrt{\frac{16N_c}{\beta_0(Y + \lambda)}} \right]. \quad (45)$$

The final numerical expressions for the mean and maximum peak positions, evaluated for  $n_f = 5$  quark flavours, read:

$$\bar{\xi}(Y) = 0.5Y + 0.592722 \left( \sqrt{Y + \lambda} - \sqrt{\lambda} \right) + 0.002 \ln \frac{Y + \lambda}{\lambda}, \quad (46)$$

$$\xi_{\max}(Y) = 0.5Y + 0.592722 \left( \sqrt{Y + \lambda} - \sqrt{\lambda} \right) - \frac{1}{2} \sigma s + 0.002 \ln \frac{Y + \lambda}{\lambda}. \quad (47)$$

**Width.** The DG distribution dispersion  $\sigma$  follows from its definition in Eq. (38) for  $n = 2$ . The full expression for the second moment  $K_2(Y, \lambda)$  can be found in Appendix B, Eq. (118), from which taking the squared root, followed by the Taylor expansion in  $(1/\sqrt{y + \lambda})$  or  $\sqrt{\alpha_s}$  and keeping trace of all terms in  $(1/(y + \lambda))$  or  $\alpha_s$ , the NMLLA+NLO\* expression for the width is obtained:

$$\sigma(Y, \lambda) = \left( \frac{\beta_0}{144N_c} \right)^{1/4} \sqrt{(Y + \lambda)^{3/2} - \lambda^{3/2}} \left\{ 1 - \frac{\beta_0}{64} f_1(Y, \lambda) \sqrt{\frac{16N_c}{\beta_0(Y + \lambda)}} + \left[ \frac{9}{16} a_2 f_2(Y, \lambda) - \frac{3}{64} \left( \frac{3a_1^2}{16N_c^2} f_2(Y, \lambda) + \frac{a_1\beta_0}{8N_c^2} f_2(Y, \lambda) - \frac{\beta_0^2}{64N_c^2} f_2(Y, \lambda) + \frac{3\beta_0^2}{128N_c^2} f_1^2(Y, \lambda) \right) + \frac{\beta_1}{64\beta_0} (\ln 2(Y + \lambda) - 2) f_3(Y, \lambda) \right] \frac{16N_c}{\beta_0(Y + \lambda)} \right\}, \quad (48)$$

where the functions  $f_i$  are also defined in Appendix B. The new correction term, proportional to  $(1/(Y + \lambda))$ , is of order  $\mathcal{O}(\alpha_s)$  and decreases the width of the distribution and so does  $\lambda$  for the truncated cascade with  $Q_0 > \Lambda_{\text{QCD}}$ . The numerical expression for the width (for  $n_f = 5$  quark flavours) reads:

$$\sigma(Y) = 0.36499 \sqrt{(Y + \lambda)^{3/2} - \lambda^{3/2}} \left\{ 1 - 0.299739 f_1(Y, \lambda) \frac{1}{\sqrt{Y + \lambda}} - [1.12479 f_2(Y, \lambda) + 0.0449219 f_1^2(Y, \lambda) + (0.32239 - 0.246692 \ln(Y + \lambda)) f_3(Y, \lambda)] \frac{1}{Y + \lambda} \right\}. \quad (49)$$

**Skewness.** The NMLLA term of the third DG moment,  $K_3$ , turns out to vanish like the leading order one [48]. According to the definition in Eq. (38), the skewness  $s = K_3 \sigma^{-3}$  presents an extra subleading term which in this resummation scheme comes from the expansion of the second contribution to  $\sigma^{-3}$ , proportional to  $1/\sqrt{(Y + \lambda)}$ , as written in Eq. (122) of Appendix B, such that

$$s(Y, \lambda) = -\frac{a_1}{16} \frac{\left( \frac{144N_c}{\beta_0} \right)^{1/4}}{\sqrt{(Y + \lambda)^{3/2} - \lambda^{3/2}}} \left[ 1 - \frac{\beta_0}{64} f_1(Y, \lambda) \sqrt{\frac{16N_c}{\beta_0(Y + \lambda)}} \right]. \quad (50)$$

In [22], only the first term of this expression was provided, the subleading contribution given here is thus new. This NMLLA+NLO\* correction to Eq. (50) increases the skewness of the distribution, while for increasing  $\lambda$  it should decrease again, thus revealing two competing effects. The net result is a displacement

of the tails of the HBP distribution downwards to the left and upwards to the right from the peak position and depending on the sign given by both effects (Fig. 2). The final numerical expression for the skewness (for  $n_f = 5$  quark flavours) reads:

$$s(Y) = -\frac{1.94704}{\sqrt{(Y+\lambda)^{3/2} - \lambda^{3/2}}} \left[ 1 - 0.299739 f_1(Y, \lambda) \frac{1}{\sqrt{Y+\lambda}} \right]. \quad (51)$$

**Kurtosis.** The evolution of the kurtosis follows from the expressions for the fourth DG moment, given in Eqs. (120) and (123) of Appendix B. As shown in the same appendix, the proper Taylor expansion in powers of  $(1/\sqrt{Y+\lambda})$  which keeps trace of higher-order corrections and leads to:

$$\begin{aligned} k(Y, \lambda) = & -\frac{27}{5(Y+\lambda)} \sqrt{\frac{\beta_0(Y+\lambda)}{16N_c}} \frac{1 - \left(\frac{\lambda}{Y+\lambda}\right)^{5/2}}{\left[1 - \left(\frac{\lambda}{Y+\lambda}\right)^{3/2}\right]^2} \left\{ 1 + \frac{\beta_0}{16} (f_1(Y, \lambda) - \frac{5}{3} f_4(Y, \lambda)) \sqrt{\frac{16N_c}{\beta_0(Y+\lambda)}} \right. \\ & + \left[ \left( \frac{25}{24} f_5(Y, \lambda) - \frac{9}{4} f_2(Y, \lambda) \right) a_2 + \frac{a_1^2}{256N_c^2} \left( 9f_2(Y, \lambda) - \frac{25}{2} f_5(Y, \lambda) \right) \right. \\ & + \frac{a_1\beta_0}{256N_c^2} (6f_2(Y, \lambda) - 5f_5(Y, \lambda)) + \frac{\beta_0^2}{256N_c^2} \left( -\frac{3}{4} f_2(Y, \lambda) + \frac{54}{8} f_1^2(Y, \lambda) + \frac{275}{24} f_5(Y, \lambda) \right. \\ & - 15f_1(Y, \lambda)f_4(Y, \lambda)) + \frac{5\beta_1}{96\beta_0} \left( \ln 2(Y+\lambda) - \frac{2}{3} \right) f_6(Y, \lambda) \\ & \left. \left. - \frac{\beta_1}{16\beta_0} (\ln 2(Y+\lambda) - 2) f_3(Y, \lambda) \right] \frac{16N_c}{\beta_0(Y+\lambda)} \right\}, \quad (52) \end{aligned}$$

where the functions  $f_i$  can be again found in Appendix B. The new NMLLA+NLO\* correction for the kurtosis affects the distribution by making it smoother in the tails and wider in the hump region. The final numerical expression for the kurtosis (for  $n_f = 5$  quark flavours) reads:

$$\begin{aligned} k(Y) = & -\frac{2.15812}{\sqrt{Y+\lambda}} \frac{1 - \left(\frac{\lambda}{Y+\lambda}\right)^{5/2}}{\left[1 - \left(\frac{\lambda}{Y+\lambda}\right)^{3/2}\right]^2} \left\{ 1 + [1.19896 f_1(Y, \lambda) - 1.99826 f_4(Y, \lambda)] \frac{1}{\sqrt{Y+\lambda}} \right. \\ & + [1.07813 f_1^2(Y, \lambda) + 4.49915 f_2(Y, \lambda) + 1.28956 f_3(Y, \lambda) - 2.39583 f_1(Y, \lambda) f_4(Y, \lambda) \\ & - 3.76231 f_5(Y, \lambda) + 0.0217751 f_6(Y, \lambda) \\ & \left. - (0.986767 f_3(Y, \lambda) - 0.822306 f_6(Y, \lambda)) \ln(Y+\lambda)] \frac{1}{Y+\lambda} \right\}. \quad (53) \end{aligned}$$

**Final DG expression.** The final expression of the DG parametrisation of the single inclusive distribution of soft hadrons inside gluon and quark jets, Eq. (35), can be obtained summing all its individually-derived NMLLA+NLO\*-resummed components: the mean multiplicity  $\mathcal{N}(Y, \lambda)$  Eq. (40), the mean peak position  $\bar{\xi}(Y, \lambda)$  Eq. (43), the dispersion  $\sigma(Y, \lambda)$  Eq. (48), the skewness Eq.  $s(Y, \lambda)$  (50), and kurtosis  $k(Y, \lambda)$  Eq. (52). In Fig. 3, we display the resulting DG for two different values of the hadronisation parameter  $\lambda = 1.4$  ( $Y = 5.8$ ,  $Q_0 = 1$  GeV,  $\Lambda_{\text{QCD}} = 0.25$  GeV) and  $\lambda = 2.0$  ( $Y = 5.2$ ,  $Q_0 = 1$  GeV,  $\Lambda_{\text{QCD}} = 0.25$  GeV) for a jet of virtuality  $Q = 350$  GeV and reconstructed jet energy  $E = 500$  GeV inside a radius cone  $\theta = 0.7$ . The distribution is compared to the corresponding MLLA predictions with the Fong-Webber results from [22] after setting to zero all terms proportional to  $1/Y$  in the same expressions.

The contributions from the set of NMLLA+NLO\* corrections to the MLLA DG appear to be quite substantial and decrease for increasing  $\lambda$ , since  $\lambda$  guarantees the convergence of the perturbative series

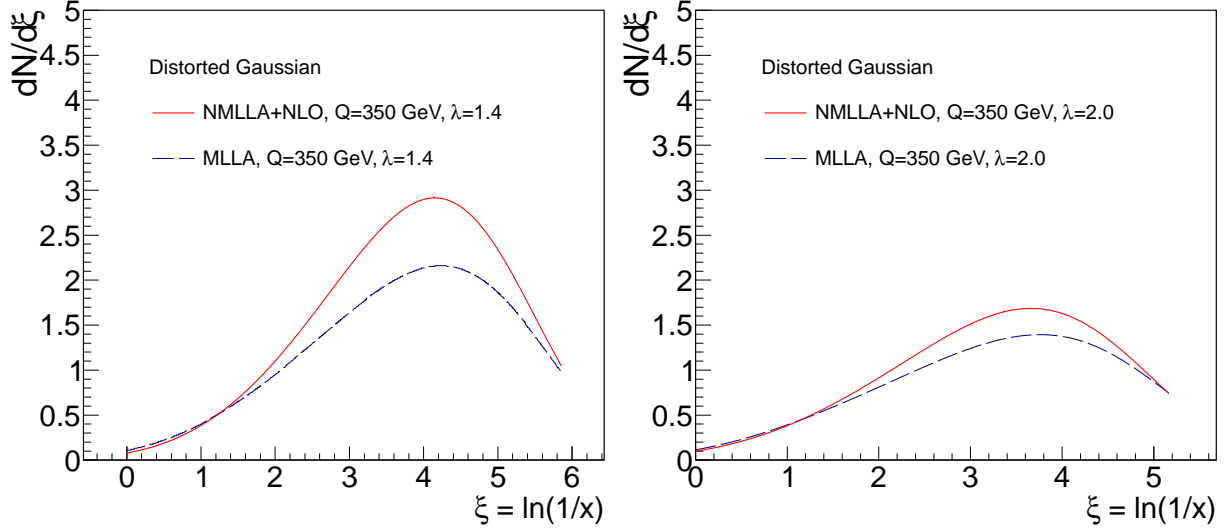


Figure 3: Comparison of the distorted Gaussian hadron distributions obtained for a jet of virtuality  $Q = 350$  GeV evolved using NMLLA+NLO\* (solid curve) and MLLA (dashed curve) equations, for two hadronisation parameters:  $\lambda = 1.4$  (left) and  $\lambda = 2.0$  (right).

for  $Q_0 \gg \Lambda_{\text{QCD}}$ . Physically, for higher values of the shower energy cut-off  $Q_0$ , the strength of the coupling constant decreases and the probability for the emission of soft gluon bremsstrahlung decreases accordingly, making the multiplicity distribution and the peak position smaller. The difference between the MLLA and NMLLA+NLO\* resummed distributions is, as mentioned above, mainly due to running-coupling effects, proportional to  $\beta_1$ , at large  $\xi$  (small  $x$ ) which is not unexpected because in this region they are more pronounced due to the  $\ln(xE\theta)$  dependence in the denominator of the strong coupling. On the other hand, energy conservation plays a more important role in the hard fragmentation region  $x \sim 1$  ( $\xi \sim 0$ ), where the NMLLA+NLO\* DG is somewhat suppressed compared with the MLLA DG.

### 3.3 Multiplicities for the single inclusive $D_g$ and $D_q$ distributions

In this section we determine the coefficient function involved in Eq. (25a) that provide higher-order corrections to the quark/gluon multiplicity ratio. As shown through Eq. (28), the  $\mathcal{D}^-(\omega, \lambda)$  component is negligible and thus the solutions for the gluon and quark single inclusive distributions can be directly obtained from  $\mathcal{D}^+$  in the form

$$\mathcal{D}_q(\omega, Y, \lambda) \approx C_q^g(\Omega) \mathcal{D}^+(\omega, Y, \lambda), \quad C_q^g(\Omega) = \frac{P_{qg}(\Omega)}{P_{++}(\Omega) - P_{--}(\Omega)}, \quad (54a)$$

$$\mathcal{D}_g(\omega, Y, \lambda) \approx C_g^g(\Omega) \mathcal{D}^+(\omega, Y, \lambda), \quad C_g^g(\Omega) = \frac{P_{++}(\Omega) - P_{qg}(\Omega)}{P_{++}(\Omega) - P_{--}(\Omega)}. \quad (54b)$$

Making use of the expressions (20a)–(20d) and (22a)–(22b), and expanding in  $\omega$  results in

$$C_q^g(\Omega) \approx \frac{C_F}{N_c} \left[ 1 + c_q^{(0)} \Omega + c_q^{(1)} \Omega^2 + \mathcal{O}(\Omega^3) \right], \quad C_g^g(\Omega) \approx 1 + c_g^{(0)} \Omega + c_g^{(1)} \Omega^2 + \mathcal{O}(\Omega^3), \quad (55)$$

where the numerical values of the constants, for  $n_f = 5$  quark flavours, read

$$c_q^{(0)} = \frac{a_1 - b_1}{4N_c} - \frac{3}{4} \stackrel{n_f=5}{=} -0.049, \quad (56)$$

$$c_q^{(1)} = \frac{7}{8} + \frac{a_1 - b_1}{16N_c} \left( \frac{a_1 - b_1}{N_c} - 3 \right) + \frac{C_F}{N_c} b_2 - a_2 \stackrel{n_f=5}{=} 0.608, \quad (57)$$

$$c_g^{(0)} = -\frac{b_1}{4N_c} \stackrel{n_f=5}{=} -0.247, \quad (58)$$

$$c_g^{(1)} = \frac{b_1}{16N_c^2} (b_1 - a_1) + \frac{C_F}{N_c} \left( b_2 - \frac{5}{8} + \frac{\pi^2}{6} \right) \stackrel{n_f=5}{=} 0.045. \quad (59)$$

The  $c_i^{(0)}$  numerical constants in Eq. (55) were obtained in [4]. Performing the inverse Mellin-transform back to the  $x$ -space, or making the equivalent replacement  $\Omega \rightarrow \frac{\partial}{\partial \xi} + \frac{\partial}{\partial Y}$ , one has

$$D_q(\xi, Y, \lambda) \approx \frac{C_F}{N_c} \left[ 1 + c_q^{(0)} \left( \frac{\partial}{\partial \xi} + \frac{\partial}{\partial Y} \right) + c_q^{(1)} \left( \frac{\partial}{\partial \xi} + \frac{\partial}{\partial Y} \right)^2 \right] D^+(\xi, Y, \lambda), \quad (60a)$$

$$D_g(\xi, Y, \lambda) \approx \left[ 1 + c_g^{(0)} \left( \frac{\partial}{\partial \xi} + \frac{\partial}{\partial Y} \right) + c_g^{(1)} \left( \frac{\partial}{\partial \xi} + \frac{\partial}{\partial Y} \right)^2 \right] D^+(\xi, Y, \lambda), \quad (60b)$$

which in a more compact form can be rewritten as

$$D_a(\xi, Y, \lambda) \approx \frac{C_A}{N_c} \left[ D^+(\xi, Y, \lambda) + c_A^{(0)} \left( \frac{\partial D^+(\xi, Y, \lambda)}{\partial \xi} + \frac{\partial D^+(\xi, Y, \lambda)}{\partial Y} \right) + c_A^{(1)} \left( \frac{\partial^2 D^+(\xi, Y, \lambda)}{\partial \xi^2} + 2 \frac{\partial^2 D^+(\xi, Y, \lambda)}{\partial \xi \partial Y} + \frac{\partial^2 D^+(\xi, Y, \lambda)}{\partial Y^2} \right) \right] \quad (61)$$

for numerical considerations. The first and second derivatives in Eqs. (60a) and (60b) can be evaluated numerically. They provide corrections which are suppressed for the first and second terms of orders  $\mathcal{O}(\sqrt{\alpha_s})$  and  $\mathcal{O}(\alpha_s)$  respectively. In Fig. 4, we compare the quark ( $D_q$ ), gluon ( $D_g$ ) and parton ( $D^+$ ) hadron spectra obtained in the MLLA (left) and NMLLA-NLO\* (right) schemes for a jet of virtuality  $Q = 350$  GeV and hadronisation parameter  $\lambda = 1.4$ . The NMLLA-NLO\* distributions are obtained from the above Eqs. (60a), (60b) and (35), while the MLLA are obtained setting to zero  $c_q^{(1)}$  and  $c_g^{(1)}$  in Eqs. (60a) and (60b) respectively and removing the  $\mathcal{O}(\alpha_s)$  corrections in (35) for  $D^+(\xi, Y)$ .

A clear difference is observed in the quark and gluon jet initiated distributions given by the colour factor  $C_F/N_c = 4/9$  and the role of higher-order corrections which prove more sizable for the NMLLA+NLO\* scheme over the whole phase space  $0 \leq \xi \leq Y$ , as observed in the right panel of Fig. 4. In [4] however, the role of  $\mathcal{O}(\sqrt{\alpha_s})$  corrections, proportional to  $c_q^{(0)}$  and  $c_g^{(0)}$  in Eqs. (60a) and (60b), was reabsorbed into the inclusive spectrum  $D^+(\xi, Y)$  through a shift to a slightly different jet energy  $E_A = E \exp(c_A^{(0)})$ , which allowed for a direct comparison between the MLLA  $D^+(\xi, Y)$  and the hadronic energy-momentum spectrum (for a complete review see [10]). Asymptotically ( $Q \rightarrow \infty$ ), the solution of the original Eq. (61) has a Gaussian shape near its maximum:

$$D_a(\xi, Q^2) \approx \frac{C_A}{N_c} \frac{\mathcal{N}}{\sigma \sqrt{2\pi}} \exp \left[ -\frac{1}{2\sigma^2} (\xi - \bar{\xi})^2 \right], \quad (62)$$

normalised by the inverse asymptotic value of the mean multiplicity ratio  $r^{-1} = C_F/N_c$  in a quark jet. The ratio of gluon and quark multiplicities can be recovered by replacing  $\omega = 0$  ( $\frac{\partial}{\partial \xi} = 0$ ) in Eqs. (60a)



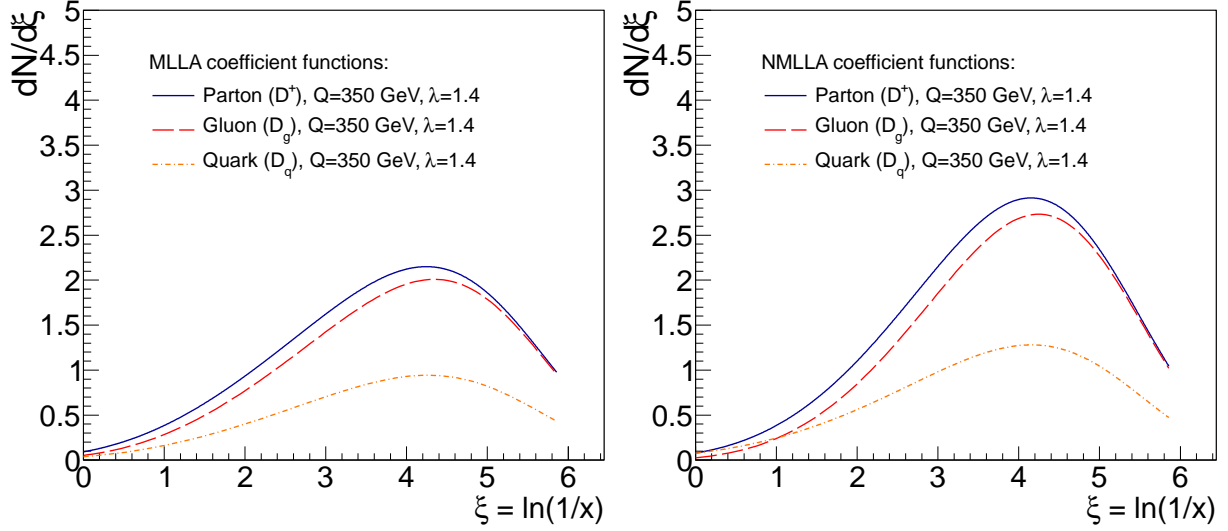


Figure 4: Comparison of the quark Eq. (60a), gluon Eq. (60b), and parton  $\mathcal{D}^+(\xi, Y)$  Eq. (35), distributions of hadrons for a jet of virtuality  $Q = 350$  GeV and hadronisation parameter  $\lambda = 1.4$  evolved using MLLA (left) and NMLLA+NLO\* (right) equations.

and (60b), such that, after expanding the result in powers of  $\sqrt{\alpha_s}$ , one is left with

$$r = \frac{\mathcal{N}_g}{\mathcal{N}_q} = \frac{N_c}{C_F} (1 - r_1 \gamma_0 - r_2 \gamma_0^2), \quad (63)$$

where, as a result of the expansion,

$$r_1 = c_q^{(0)} - c_g^{(0)} = \frac{a_1}{4N_c} - \frac{3}{4}, \quad (64)$$

$$r_2 = c_q^{(1)} - c_g^{(1)} - r_1 c_q^{(0)} - \frac{r_1}{8N_c} \left( a_1 - \frac{\beta_0}{2} \right) = \tilde{a}_2 - a_2 + r_1 \left( \frac{3}{4} - \frac{a_1}{8N_c} + \frac{\beta_0}{16N_c} \right), \quad (65)$$

with

$$\tilde{a}_2 = \frac{7}{8} + \frac{C_F}{N_c} \left( \frac{5}{8} - \frac{\pi^2}{6} \right).$$

Notice that up to the order  $\mathcal{O}(\alpha_s)$ , the multiplicity ratio does not involve corrections proportional to  $\beta_1$ , which only appear beyond this level of accuracy [20]. Up to the NMLLA order in  $\mathcal{O}(\alpha_s)$ , Eq. (63) coincides with the expression found in [49], which gives further support to the calculations carried out in our work. A more updated evaluation of the mean multiplicity ratio, including two-loop splitting functions, was given recently in [21].

### 3.4 Limiting spectrum for the DG parametrisation

The so-called limiting spectrum,  $\lambda \rightarrow 0$ , implies pushing the validity of the partonic evolution equations down to (non-perturbative) hadronisation scales,  $Q_0 \approx \Lambda_{\text{QCD}}$  [1]. Such an approach provides a minimal (and successful) approach with predictive power for the measured experimental distributions. We derive here the evolution of the distorted Gaussian moments for this limit which involves formulæ depending only on  $\Lambda_{\text{QCD}}$  as a single parameter.

**Multiplicity.** Among the various moments of the DG parametrisation, only its integral (representing the total hadron multiplicity) needs an extra free parameter to fit the data. The “local parton hadron duality” (LPHD) hypothesis is a powerful assumption which states that the distribution of partons in inclusive processes is identical to that of the final hadrons, up to an overall normalization factor, i.e. that the mean multiplicity of the measured charged hadrons is proportional to the partonic one through a constant  $\mathcal{K}^{\text{ch}}$ ,

$$\mathcal{N}^{\text{ch}}(Y) = \mathcal{K}^{\text{ch}} \mathcal{N}(Y).$$

Thus, in the limiting spectrum the mean multiplicity reads

$$\begin{aligned} \mathcal{N}^{\text{ch}}(Y) = \mathcal{K}^{\text{ch}} \exp \left\{ \sqrt{\frac{16N_c}{\beta_0}} Y - \left( \frac{a_1}{\beta_0} - \frac{1}{2} \right) \ln \sqrt{Y} - \frac{2N_c}{\beta_0} \left[ a_2 + \frac{1}{4} \left( \frac{a_1}{4N_c} \right)^2 + \frac{1}{2} \frac{a_1 \beta_0}{16N_c^2} \right. \right. \\ \left. \left. + \frac{3}{16} \left( \frac{\beta_0}{4N_c} \right)^2 - \frac{\beta_1}{4N_c \beta_0} (\ln 2Y + 2) \right] \sqrt{\frac{16N_c}{\beta_0 Y}} \right\}, \end{aligned} \quad (66)$$

which is in agreement with the mean multiplicity first found in [20], supported by the improved solution of the evolution equations accounting for the same set of corrections.

**Peak position.** For the limiting spectrum, the mean peak position Eq. (43) can be approximated as follows:

$$\bar{\xi} = \frac{Y}{2} + \frac{a_1}{16N_c} \sqrt{\frac{16N_c}{\beta_0}} Y - 2N_c \frac{a_2}{\beta_0} \ln Y \quad (67)$$

thanks to the fortuitous smallness  $\mathcal{O}(10^{-3})$  of the NMLLA correction to  $\bar{\xi}$  at high-energy where  $Y + \lambda \gg \lambda$ . Notice that, as shown in [22], the MLLA version of Eq. (67) up to the second order is finite. The origin of the third  $\propto \ln Y$  correction in this resummation framework comes from the truncated expansion of the anomalous dimension Eq. (34) in  $\mathcal{O}(\alpha_s)$ , which is proportional to  $1/Y$  by making  $(-\partial \gamma_\omega / \partial \omega)$  at  $\omega = 0$ , and hence yields the  $\propto \ln Y$  term after integrating over  $Y$ . Therefore, we assume that Eq. (67) is valid for  $Q \gg Q_0 \approx \Lambda_{\text{QCD}}$ .

The maximum of the peak position for the limiting spectrum DG can be obtained via Eq. (44) which involves the mean peak position as well as the other higher-order moments. In a generic form, the moments of the distorted Gaussian associated with the dispersion (48), skewness (50), kurtosis (52), and  $k_5$  (45), are finite for  $n \geq 2$  for the limiting spectrum and can be written as

$$\begin{aligned} K_n(\alpha_s(Y + \lambda), \alpha_s(\lambda)) \simeq \alpha_s(Y + \lambda)^{-(n+1)/2} \left[ \mathcal{K}_n^{(0)} + \mathcal{K}_n^{(0)} \sqrt{\alpha_s(Y + \lambda)} + \mathcal{K}_n^{(0)} \alpha_s(Y + \lambda) \right. \\ \left. - \{ \alpha_s(Y + \lambda) \Leftrightarrow \alpha_s(\lambda) \} \right], \end{aligned} \quad (68)$$

where the constants  $\mathcal{K}_n^{(0)}$  and the functions  $f_i(\lambda \rightarrow 0) \rightarrow 1$  are written in Appendix B. In other words, the second  $\lambda$ -dependent part of  $K_n$  in Eq. (68) can be dropped as  $\lambda \rightarrow 0$  for sufficiently high energy scales,  $Y + \lambda \gg \lambda$ , where  $\alpha_s(Y + \lambda) \ll \alpha_s(\lambda)$  in the r.h.s. of Eq. (68). Performing the same approximation in Eq. (68) as  $\lambda \rightarrow 0$ , the expressions for the rest of moments of the fragmentation functions in the limiting spectrum are derived below. Thus inserting Eqs. (70a), (70b), (70c) and (70d) into (44), we obtain :

$$\xi_{\text{max}} - \bar{\xi} = \frac{1}{32} a_1 \left( 1 + \frac{5}{64} \beta_0 \sqrt{\frac{16N_c}{\beta_0 Y}} \right), \quad \xi_m - \bar{\xi} = \frac{1}{96} a_1 \left( 1 + \frac{19}{320} \beta_0 \sqrt{\frac{16N_c}{\beta_0 Y}} \right) \quad (69)$$

**Width.** The width of the DG distribution in the limiting spectrum is obtained from Eq. (48):

$$\sigma(Y) = \sqrt{\frac{1}{3}Y} \left( \frac{\beta_0 Y}{16N_c} \right)^{1/4} \left\{ 1 - \frac{\beta_0}{64} \sqrt{\frac{16N_c}{\beta_0 Y}} + \left[ \frac{9}{16} a_2 - \frac{3}{64} \left( \frac{3}{16N_c^2} a_1^2 + \frac{a_1 \beta_0}{8N_c^2} + \frac{\beta_0^2}{128N_c^2} \right) + \frac{\beta_1}{64\beta_0} (\ln 2Y - 2) \right] \frac{16N_c}{\beta_0 Y} \right\}. \quad (70a)$$

**Skewness.** The skewness of the DG distribution in the limiting spectrum reads, from Eq. (50),

$$s(Y) = -\frac{a_1}{16} \sqrt{\frac{3}{Y}} \left( \frac{16N_c}{\beta_0 Y} \right)^{1/4} \left( 1 - \frac{\beta_0}{64} \sqrt{\frac{16N_c}{\beta_0 Y}} \right), \quad (70b)$$

**Kurtosis.** The kurtosis can be derived from Eq. (52):

$$k(Y) = -\frac{27}{5Y} \sqrt{\frac{\beta_0 Y}{16N_c}} \left\{ 1 - \frac{\beta_0}{24} \sqrt{\frac{16N_c}{\beta_0 Y}} - \left[ \frac{29}{24} a_2 + \left( \frac{7}{512N_c^2} a_1^2 - \frac{a_1 \beta_0}{256N_c^2} - \frac{59}{6144N_c^2} \beta_0^2 \right) + \frac{\beta_1}{96\beta_0} \left( \ln 2Y - \frac{26}{3} \right) \right] \frac{16N_c}{\beta_0 Y} \right\}. \quad (70c)$$

Accordingly, we give the last component,  $k_5$ , following from Eq. (45):

$$k_5(Y) = \frac{9}{16} a_1 \left( \frac{3}{Y} \right)^{3/2} \left( \frac{\beta_0 Y}{16N_c} \right)^{1/4} \left( 1 + \frac{85}{576} \beta_0 \sqrt{\frac{16N_c}{\beta_0 Y}} \right). \quad (70d)$$

**Final DG (limiting spectrum) expression.** In order to get the DG in the limiting spectrum, one should replace Eqs. (66)–(70c) into Eq. (35). We note that in our NMLLA+NLO\* framework, the  $\mathcal{K}^{\text{ch}}$  from the DG can be smaller than that found in [20] since it should fix the right normalisation enhanced by second-loop coupling constant effects. Notice also that setting subleading corrections to zero, we recover the results from [22] as expected. In Fig. 5, the MLLA and NMLLA+NLO\* distorted Gaussians are displayed in the limiting spectrum approximation for a jet virtuality  $Q = 350$  GeV in the interval  $0 \leq \xi \leq Y$ , for  $Y = 7.5$ .

We can see a sizable difference between the MLLA  $D^+(\xi, Y)$  and the NMLLA+NLO\*  $D^+(\xi, Y)$  evolutions, which is mainly driven by the two-loop  $\propto \beta_1$  correction in the mean multiplicity and other moments of the DG, as mentioned above. The account of energy conservation can be observed at low  $\xi$ , i.e. for harder partons. Similar effects have been discussed in [50] where an exact numerical solution of the MLLA evolution equations was provided with one-loop coupling constant. Numerical solutions of exact MLLA equations provide a perfect account of energy conservation at every splitting vertex of the branching process in the shower. For this reason, accounting for higher-order corrections  $\mathcal{O}(\alpha_s^{n/2})$  to the truncated series of the single inclusive spectrum of hadrons should follow similar features and trends to that provided by the numerical solutions of [50] (see also [51]), although our NMLLA+NLO\* solution incorporates in addition the two-loop coupling constant.

In Fig. 6 we display the same set of curves as in the Fig. 4 with the right normalisation given by the coefficient functions for quark and gluon jets. The overall corrections provided by the coefficient functions slightly decrease the normalisation of the spectrum in a gluon jet as well as its width  $\sigma$ . In the quark jet, upon normalisation by the colour factor  $C_F/N_c$ , the normalisation is decreased while the

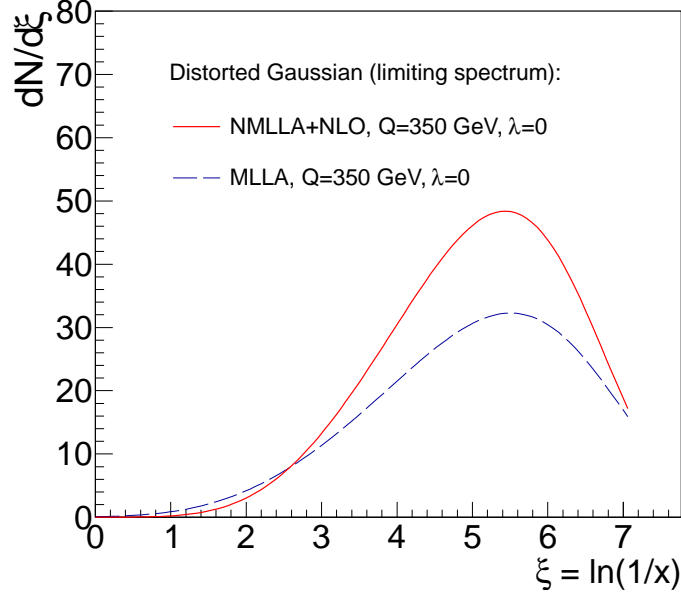


Figure 5: Comparison of the distorted Gaussian hadron distributions obtained for a jet of virtuality  $Q = 350$  GeV evolved using MLLA and NMLLA+NLO\* equations, in the limiting spectrum (i.e.  $Q_0 = \Lambda_{\text{QCD}}$ , hadronisation parameter  $\lambda = 0$ ).

width is slightly enlarged. In order to better visualise the less trivial enlargement for the width, we can for instance consider  $e^+e^-$ -annihilation into hadrons at the LEP-2 centre of mass energy  $\sqrt{s} = 196$  GeV for a quark jet of virtuality  $Q = \sqrt{s}/2 = 98$  GeV with  $Y = \ln(\sqrt{s}/(2\Lambda_{\text{QCD}})) \approx 6.0$  for  $\Lambda_{\text{QCD}} = 0.25$  GeV. If the resulting distribution  $D_q(\xi, Y)$  is refitted to a DG and compared with the  $D^+(\xi, Y)$ , the enlargement of the width compared with that given by  $D^+$  (70a) can reach 10%. This latter effect is mainly due to the positive  $\mathcal{O}(\alpha_s)$  correction to the coefficient function  $C_q^g$  given by the larger numerical coefficient  $c_q^{(0)} = 0.487$ . Similar effects have been discussed in [50]. In conclusion, we will directly fit the  $D^+(\xi, Y)$  distribution to the data of final state hadrons in the limiting spectrum approximation.

### 3.5 Higher-order corrections for the DG limiting spectrum

The exact solution of the MLLA evolution equations with one-loop coupling constant entangles corrections which go beyond  $\mathcal{O}(\sqrt{\alpha_s})$ , though the equations are originally obtained in this approximation [5]. The exact solution resums fast convergent Bessel series in the limiting spectrum  $\lambda \rightarrow 0$ . Using the DG parametrisation it is possible to match the exact solution in the vicinity of the peak position  $\delta \ll 1$  after determining the DG moments:  $\xi_1 = \bar{\xi}$ ,  $\xi_2 = \langle \xi^2 \rangle$ ,  $\xi_3 = \langle \xi^3 \rangle$ ,  $\xi_4 = \langle \xi^4 \rangle$ , related to the dispersion, skewness and kurtosis through [52]:

$$\sigma^2 = \xi_2 - \bar{\xi}^2, \quad (71)$$

$$s = \frac{1}{\sigma^3}(\xi_3 - 3\xi_2\bar{\xi} + 2\bar{\xi}^3), \quad (72)$$

$$k = \frac{1}{\sigma^4}(\xi_4 - 4\xi_3\xi_1 - 3\xi_2^2 + 12\xi_2\bar{\xi}^2 - 6\bar{\xi}^4), \quad (73)$$

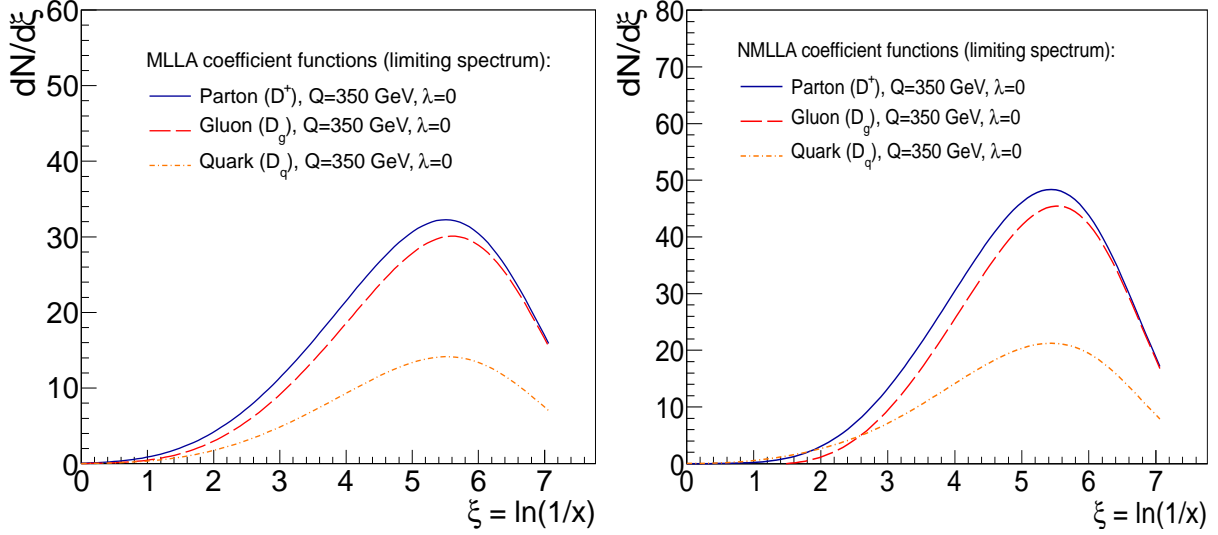


Figure 6: Comparison of the distorted Gaussian hadron distributions obtained for a quark Eq. (60a), gluon Eq. (60b), and  $D^+(\xi, Y)$  Eq. (35), for a jet of virtuality  $Q = 350$  GeV evolved using MLLA (left) and NMLLA+NLO\* (right) equations, in the limiting spectrum (i.e.  $Q_0 = \Lambda_{\text{QCD}}$ , hadronisation parameter  $\lambda = 0$ ).

where  $\xi_n$  is determined via

$$\xi_n = Y^n \cdot \mathcal{L}_n(B+1, B+2, z), \quad B = \frac{a_1}{\beta_0}, \quad z = \sqrt{\frac{16N_c}{\beta_0}} Y \quad (74)$$

discussed in more detail in Appendix C. Similarly, these extra corrections, which better account for energy conservation and provide an improved description of the shape of the inclusive hadron distribution in jets, will be computed and added hereafter to all the NMLLA+NLO\* DG moments, as it was done in [4] for the particular case of the mean peak position,  $\bar{\xi}$ , but extended here also to all other components: Eqs. (67), (70a), (70b) and (70c).

**Multiplicity.** The extra “hidden” corrections discussed in Appendix C result in one extra term for the multiplicity in the DG limiting spectrum, which is inversely proportional to  $Y$  and amounts to:

$$\Delta\mathcal{N} = -\frac{0.168007}{Y}, \quad \text{for } n_f = 3, \text{ and } \quad \Delta\mathcal{N} = -\frac{0.23252}{Y}, \quad \text{for } n_f = 5. \quad (75)$$

However, we can use directly the full-NLO result obtained in [20] for the multiplicity. In this case the extra correction amounts to:

$$\Delta\mathcal{N} = -(0.08093 + 0.16539 \ln Y) \frac{1}{Y}, \quad \text{for } n_f = 3, \text{ and} \quad (76)$$

$$\Delta\mathcal{N} = -(0.00068 - 0.161658 \ln Y) \frac{1}{Y}, \quad \text{for } n_f = 5. \quad (77)$$

although the terms  $\propto \frac{1}{\sqrt{Y}}$  and  $\propto \frac{1}{Y}$  are almost constant and practically compensate to each other at the currently accessible energies.

**Peak position.** The mean peak value of the DG distribution,  $\bar{\xi}$ , truncated as done in Eq. (43) can be improved as discussed in [4]. The NMLLA correction proportional to  $\ln Y$  is of relative order  $\mathcal{O}(\sqrt{\alpha_s})$  and is very small  $\mathcal{O}(10^{-3} \ln Y)$  compared to the second term. There is one extra correction (numerical constant) to  $\bar{\xi}$  coming from the exact solution of Eq. (26) with  $a_2 = 0$ , written in terms of Bessel series in Appendix C. Indeed, substituting Eq. (135) into (133) (see Appendix C for a complete derivation), one obtains the extra NMLLA term to  $\bar{\xi}$ :

$$\Delta\bar{\xi} = -\frac{\beta_0}{32N_c}B(2B+3), \quad (78)$$

from the expansion of the Bessel series through the Eq. (133) that should be added to Eq. (43). Therefore, the full resummed expression of the mean peak position reads

$$\bar{\xi} = \frac{Y}{2} + \frac{a_1}{16N_c} \sqrt{\frac{16N_c}{\beta_0}} Y - 2N_c \frac{a_2}{\beta_0} \ln Y - \frac{a_1(2a_1 + 3\beta_0)}{32N_c\beta_0} \quad (79)$$

in its complete NMLLA+NLO\* form. The corresponding position of the maximum is related to the mean peak value by the expression [48]:

$$\xi_{\max} - \bar{\xi} = -\frac{1}{2}\sigma s = \frac{3a_1}{32N_c}, \quad (80)$$

such that

$$\xi_{\max} = \frac{Y}{2} + \sqrt{\frac{a_1^2}{16N_c\beta_0}} Y - 2N_c \frac{a_2}{\beta_0} \ln Y - \frac{a_1^2}{16N_c\beta_0}. \quad (81)$$

where the DLA width  $\sigma$  and skewness  $s$  are enough for the computation. Asymptotically ( $Y \rightarrow \infty$ ) and factorising by  $Y$ , one recovers the maximum of the peak position for the DLA spectrum Eq. (1). In the same approximation, since  $s(Y) \rightarrow 0$ , the expression of the mean peak position in Eq. (80) coincides with that of the maximum of the Gaussian distribution. Of course, the ensemble of NMLLA corrections written in Eq. (79) can be obtained from Eq. (26), provided that one can determine the exact solution of the evolution equations. Notice that Eq. (81) does not include any term  $\propto \beta_1$ , as this kind of term appears when higher-order corrections are included in the evolution equations and their solutions.

**Width.** Similar extra corrections can be found for the dispersion by calculating  $\xi_2$  through this recursive procedure. By making use of Eq. (74) and the full derivation presented in Appendix C, it was found in [52]:

$$\frac{\xi_2}{Y^2} = \frac{1}{4} + \frac{B(B+\frac{1}{3})}{z^2} + \frac{(B+\frac{1}{3})}{z^2} \left(1 - \frac{2B(B+2)}{z^2}\right) \frac{I_{B+2}(z)}{I_{B+1}(z)}, \quad (82)$$

such that, with  $\sigma^2 = \xi_2 - \bar{\xi}^2$  given by Eq. (71), one finds the extra correction (for  $n_f = 5$ )

$$\frac{\Delta\sigma}{0.36499Y^{3/4}} = \frac{1.98667}{Y^{3/2}}, \quad (83)$$

which should be accordingly added to the r.h.s. of Eq. (70a).

**Skewness.** In the case of the skewness, the expression for  $\xi_3$  reads

$$\frac{\xi_3}{Y^3} = \frac{1}{8} + \frac{3B(B+1)}{2z^2} \left( 1 - \frac{4B(B+3)}{3z^2} \right) + \frac{2}{z} \left[ \frac{3B+2}{8} - \frac{B(B+1)(B+3)}{z^2} \left( 1 - \frac{2B(B+2)}{z^4} \right) \right] \frac{I_{B+2}(z)}{I_{B+1}(z)} \quad (84)$$

such that, if one makes use of the expression (72), the extra correction reads (for  $n_f = 5$ )

$$\frac{\Delta s}{-1.94703/Y^{3/4}} = -\frac{1.64393}{Y}, \quad (85)$$

to be added to the r.h.s. of Eq. (70b). Notice that Eq. (84) was given in [52] without accounting for terms  $\mathcal{O}(z^{-4})$  and  $\mathcal{O}(z^{-7})$ . Such terms cannot be neglected when dealing with MLLA and NMLLA corrections.

**Kurtosis.** Finally, for the kurtosis, we obtain the formula for  $\xi_4$ :

$$\begin{aligned} \frac{\xi_4}{Y^4} = & \frac{1}{16} - \frac{(B+4)(15B^3 + 30B^2 + 5B - 2)}{5z^2} \left( 1 - \frac{4B(B+3)}{3z^4} \right) + \frac{9B^2 + 15B + 2}{6z^2} \\ & + \frac{1}{z} \left[ \frac{B+1}{2} + \frac{4(B+3)(B+4)(15B^3 + 30B^2 + 5B - 2)}{15z^4} \left( 1 - \frac{2B(B+2)}{z^2} \right) \right. \\ & \left. - \frac{5B^3 + 35B^2 + 50B + 8}{5z^2} \right] \frac{I_{B+2}(z)}{I_{B+1}(z)}, \end{aligned} \quad (86)$$

which can be cast into Eq. (73) to obtain the corresponding correction which reads (for  $n_f = 5$ ):

$$\frac{\Delta k}{-2.15812/\sqrt{Y}} = -\frac{8.05771}{Y^{3/2}}, \quad (87)$$

to be also added to Eq. (70c).

**Final numerical formulæ.** For easiness of comparison to the data, we provide here the final numerical expressions for the energy evolution of the NMLLA+NLO\* components of DG hadron distribution of jets in the limiting spectrum, evaluated from Eqs. (66), (67), (70a), (70b) and (70c) plus the higher-order corrections eqs. (77), (78), (83), (85) and (87). We include the expressions for  $n_f = 3, 4, 5$  active quark flavours, although only the cases  $n_f = 4, 5$  are relevant for most phenomenological applications (jets are usually measured with energies (well) above the charm and bottom-quark mass thresholds). For  $n_f = 3$  quark flavours, one finds

$$\begin{aligned} \mathcal{N}(Y) = & \mathcal{K}^{\text{ch}} \exp \left[ 2.3094\sqrt{Y} - 0.373457 \ln Y + (0.061654 + 0.456178 \ln Y) \frac{1}{\sqrt{Y}} \right. \\ & \left. + (0.121834 - 0.14749 \ln Y) \frac{1}{Y} \right], \end{aligned} \quad (88)$$

$$\bar{\xi}(Y) = 0.5Y + 0.539929\sqrt{Y} - 0.05 \ln Y, \quad (89)$$

$$\xi_{\text{max}}(Y) = 0.5Y + 0.539929\sqrt{Y} - 0.291524 - 0.05 \ln Y, \quad (90)$$

$$\sigma(Y) = 0.379918Y^{3/4} \left[ 1 - 0.324759 \frac{1}{\sqrt{Y}} - (1.6206 - 0.296296 \ln Y) \frac{1}{Y} + \frac{1.70797}{Y^{3/2}} \right], \quad (91)$$

$$s(Y) = -\frac{1.84616}{Y^{3/4}} \left[ 1 - 0.324759 \frac{1}{\sqrt{Y}} - \frac{1.63978}{Y} \right], \quad (92)$$

$$k(Y) = -\frac{2.33827}{\sqrt{Y}} \left[ 1 - 0.866025 \frac{1}{\sqrt{Y}} + (0.713767 - 0.197531 \ln Y) \frac{1}{Y} - \frac{6.99062}{Y^{3/2}} \right]. \quad (93)$$

For  $n_f = 4$  quark flavours, relevant for jet analysis above the charm mass threshold ( $m_c \approx 1.3$  GeV) but below the bottom mass, one finds

$$\begin{aligned}\mathcal{N}(Y) &= \mathcal{K}^{\text{ch}} \exp \left[ 2.4\sqrt{Y} - 0.427778 \ln Y + (0.0214879 + 0.44352 \ln Y) \frac{1}{\sqrt{Y}} \right. \\ &\quad \left. + (0.0682865 - 0.158071 \ln Y) \frac{1}{Y} \right],\end{aligned}\quad (94)$$

$$\bar{\xi}(Y) = 0.5Y + 0.564815\sqrt{Y} - 0.0287888 \ln Y, \quad (95)$$

$$\xi_{\text{max}}(Y) = 0.5Y + 0.564815\sqrt{Y} - 0.319015 - 0.0287888 \ln Y, \quad (96)$$

$$\sigma(Y) = 0.372678Y^{3/4} \left[ 1 - 0.312499 \frac{1}{\sqrt{Y}} - (1.31978 - 0.2772 \ln Y) \frac{1}{Y} + \frac{1.83441}{Y^{3/2}} \right], \quad (97)$$

$$s(Y) = -\frac{1.89445}{Y^{3/4}} \left[ 1 - 0.312499 \frac{1}{\sqrt{Y}} - \frac{1.64009}{Y} \right], \quad (98)$$

$$k(Y) = -\frac{2.25}{\sqrt{Y}} \left[ 1 - 0.833333 \frac{1}{\sqrt{Y}} + (0.740793 - 0.1848 \ln Y) \frac{1}{Y} - \frac{7.47314}{Y^{3/2}} \right]; \quad (99)$$

and for  $n_f = 5$  quark flavours relevant for jet analysis above the bottom mass threshold ( $m_b \approx 4.2$  GeV):

$$\begin{aligned}\mathcal{N}(Y) &= \mathcal{K}^{\text{ch}} \exp \left[ 2.50217\sqrt{Y} - 0.491546 \ln Y - (0.06889 - 0.41151 \ln Y) \frac{1}{\sqrt{Y}} \right. \\ &\quad \left. + (0.00068 - 0.161658 \ln Y) \frac{1}{Y} \right],\end{aligned}\quad (100)$$

$$\bar{\xi}(Y) = 0.5Y + 0.592722\sqrt{Y} + 0.002 \ln Y, \quad (101)$$

$$\xi_{\text{max}}(Y) = 0.5Y + 0.592722\sqrt{Y} - 0.351319 + 0.002 \ln Y, \quad (102)$$

$$\sigma(Y) = 0.36499Y^{3/4} \left[ 1 - 0.299739 \frac{1}{\sqrt{Y}} - (1.4921 - 0.246692 \ln Y) \frac{1}{Y} + \frac{1.98667}{Y^{3/2}} \right], \quad (103)$$

$$s(Y) = -\frac{1.94704}{Y^{3/4}} \left[ 1 - 0.299739 \frac{1}{\sqrt{Y}} - \frac{1.64393}{Y} \right], \quad (104)$$

$$k(Y) = -\frac{2.15812}{\sqrt{Y}} \left[ 1 - 0.799305 \frac{1}{\sqrt{Y}} + (0.730466 - 0.164461 \ln Y) \frac{1}{Y} - \frac{8.05771}{Y^{3/2}} \right]. \quad (105)$$

The MLLA expressions first computed in [22] can be naturally recovered from our results by keeping all terms up to  $1/\sqrt{Y}$ . For  $n_f = 5$  quark flavours, they read:

$$\mathcal{N}(Y) = \mathcal{K}^{\text{ch}} \exp \left[ 2.50217\sqrt{Y} - 0.491546 \ln Y \right], \quad (106)$$

$$\bar{\xi}(Y) = 0.5Y + 0.592722\sqrt{Y}, \quad (107)$$

$$\xi_{\text{max}}(Y) = 0.5Y + 0.592722\sqrt{Y}, \quad (108)$$

$$\sigma(Y) = 0.36499Y^{3/4} \left[ 1 - 0.299739 \frac{1}{\sqrt{Y}} \right], \quad (109)$$

$$s(Y) = -\frac{1.94704}{Y^{3/4}}, \quad (110)$$

$$k(Y) = -\frac{2.15812}{\sqrt{Y}} \left[ 1 - 0.799305 \frac{1}{\sqrt{Y}} \right], \quad (111)$$

which clearly highlight, by comparing to the corresponding full expressions above, the new NMLLA+NLO\* terms computed in this work for the first time.



### 3.6 Other corrections: finite mass, number of active flavours, power terms, and $\Lambda_{\text{QCD}}$ rescaling

**Mass effects:** In the approach discussed so far, the partons have been assumed massless and so their scaled energy and momentum spectra are identical. Experimentally, the scaled momentum distribution  $\xi_p = \ln(\sqrt{s}/(2p_h))$  is measured and, since the final-state hadrons are massive, the equivalence of the theoretical and experimental spectra no longer exactly holds. One can relate the measured  $\xi_p$  spectrum to the expected DG distribution (which depends on  $\xi \equiv \xi_E$ ) by performing the following change of variables [53]:

$$\frac{1}{\sigma_{\text{tot}}} \frac{d\sigma^h}{d\xi_p} \propto \frac{p_h}{E_h} D^+(\xi, Y), \text{ with } \xi = \ln(1/x) = \ln \left( \frac{\sqrt{s}/2}{\sqrt{(s/4)e^{-2\xi_p} + m_{\text{eff}}^2}} \right), \quad (112)$$

where the energy of a hadron with measured momentum  $p_h = (\sqrt{s}/2) \cdot \exp -\xi_p$  is  $E_h = \sqrt{p_h^2 + m_{\text{eff}}^2}$ , and  $m_{\text{eff}}$  is an effective mass of  $\mathcal{O}(\Lambda_{\text{QCD}})$  accounting for the typical mixture of pion, kaon and protons in a jet. In Fig. (7) we compare the DG distribution in the limiting-spectrum for the typical HBP of LEP-1 jets with and without mass corrections, using Eq. (112) with  $m_{\text{eff}} = 0$  and  $m_{\text{eff}} = \Lambda_{\text{QCD}} \approx 0.23$  GeV. As expected, the net effect of the non-null mass of the measured jet particles affects the tail of the distribution at high  $\xi$  (i.e. at very low momenta) but leaves otherwise relatively unaffected the rest of the distribution. In the analysis of experimental jet data in the next Section, the rescaling given by Eq. (112) will be applied to the theoretical DG distribution for values of  $m_{\text{eff}} = 0\text{--}0.35$  GeV to gauge the sensitivity of our results to finite-mass effects. Since experimentally there are not many measurements in the large  $\xi$  tail (i.e. very low particle momenta) and here the distribution has larger uncertainties than in other ranges of the spectrum, the fits to the data turn out to be rather insensitive to  $m_{\text{eff}}$ .

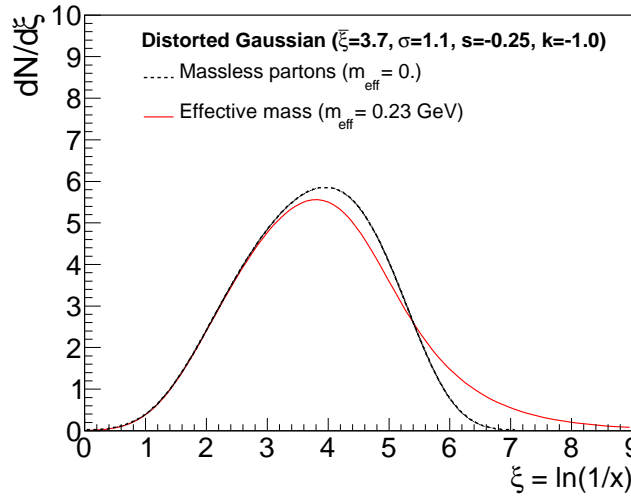


Figure 7: Comparison of the limiting-spectrum distorted Gaussian for jets typical of LEP-1 energies (mean  $\bar{\xi} = 3.7$ , width  $\sigma = 1.1$ , skewness  $s = k = -0.25$ , and kurtosis  $k = -1$ .) with and without corrections for finite-mass effects ( $m_{\text{eff}} \approx \Lambda_{\text{QCD}}$ ) according to Eq. (112).

**Number of active flavours  $n_f$ :** The available experimental  $e^+e^-$  data covers a range of jet energies  $E_{\text{jet}} \approx 1\text{--}100$  GeV which, in its lowest range, crosses the charm ( $m_c \approx 1.3$  GeV) and bottom

( $m_b \approx 4.2$  GeV) thresholds in the counting of the number of active quark flavours  $n_f$  present in the formulæ for the energy-dependence of the DG moments. Although the differences are small, rather than trying to interpolate the expressions for different values of  $n_f$  in the heavy-quark crossing regions, in what follows we will use the formulæ for  $n_f = 5$  for the evolution of all moments and rescale the obtained moments of the four lower- $\sqrt{s}$  datasets from the BES experiment [23] to account for their lower effective value of  $n_f$ . The actual numerical differences between the evolutions of the DG moments for  $n_f = 4$  and  $n_f = 5$  quark flavours – given by Eqs. (94)–(99) and (100)–(105) respectively – when evaluated for energies below the bottom-quark threshold are quite small: 0–10% for  $\mathcal{N}(Y)$ , below 1% for  $\xi_{\max}(Y)$ , around 5% for the width  $\sigma(Y)$ , and 5–10% for the skewness  $s(Y)$  and kurtosis  $k(Y)$ . In this respect, the most “robust” ( $n_f$ -insensitive) observable is the peak position of the distribution.

**Power-suppressed terms:** Power corrections of order  $\mathcal{O}(Q_0^n/Q^n)$  appear if one sets more accurate integration bounds of the integro-differential evolution equations over  $z$ , such as  $\frac{Q_0}{Q} \leq z \leq 1 - \frac{Q_0}{Q}$  instead of  $0 \leq z \leq 1$ , which actually leads to Eq. (26) after Mellin transformation with  $Q_0 \sim m_h$ , where  $m_h$  is the hadron mass (for more details see review [54, 55]). For the mean multiplicity, this type of corrections was considered in [17]. They were proved to be power-suppressed and to provide small corrections at high-energy scales. Furthermore, they become even more suppressed in the limiting spectrum case where  $Q_0$  can be extended down to  $\Lambda_{\text{QCD}}$  for infrared-safe observables like the hump-backed plateau. The MLLA computation of power corrections for differential observables is a numerical cumbersome task which, for the hump-backed plateau, would add minor improvements in the very small  $x$  domain  $\ln(1/x) \rightarrow \ln(Q/\Lambda_{\text{QCD}})$  away from the hump region of our interest, and thus they would not introduce any significant shift to the main moments of the hadron distributions (in particular its peak position  $\xi_{\max}$ , and width  $\sigma$ ).

**Rescaling of the  $\Lambda_{\text{QCD}}$  parameter:** Technically, the  $\Lambda_{\text{QCD}}$  parameter is a scheme-dependent integration constant of the QCD  $\beta$ -function. Rescaling the QCD parameter by a constant,  $\Lambda_{\text{QCD}} \rightarrow C\Lambda_{\text{QCD}}$ , would give an equally acceptable definition. In our formalism, such a variation would translate into a  $\ln C$ -shift of the constant term of the HBP peak, Eq. (81) [4], which corresponds to higher-order contributions to the solution of the evolution equations. The approach adopted here is to connect  $\Lambda_{\text{QCD}}$  to  $\alpha_s$  in the  $\overline{\text{MS}}$  factorisation scheme through the two-loop Eq. (9) and, at this level of NLO accuracy, there is no ambiguity when comparing our extracted  $\alpha_s$  results to other values obtained using the same definition.

## 4 Extraction of $\alpha_s$ from the evolution of the distribution of hadrons in jets in $e^+e^-$ collisions

In this last section, we confront our NMLLA+NLO\* calculations with all the existing charged-hadron spectra measured in jets produced in  $e^+e^-$  collisions in the range of energies  $\sqrt{s} \approx 2\text{--}200$  GeV. The experimental distributions as a function of  $\xi_p = \ln(\sqrt{s}/(2p_h))$  are fitted to the distorted Gaussian parametrisation, Eq. (35), and the corresponding DG components are derived for each dataset. More concretely, we fit the experimental distributions to the expression:

$$\frac{1}{\sigma_{\text{tot}}} \frac{d\sigma^h}{d\xi} = \mathcal{K}^{\text{ch}} \frac{2C_F}{N_c} D^+(\xi, Y), \quad (113)$$

where  $D^+(\xi, Y)$  is given by Eq. (112) corrected to take into account the finite-mass effects of the hadrons (for values of  $m_{\text{eff}} = 0\text{--}0.35$  GeV, see below) with  $Y = \ln[\sqrt{s}/(2\Lambda_{\text{QCD}})]$ . Each fit has five free parameters for the DG: maximum peak position, total multiplicity, width, skewness and kurtosis. In total, we

analyse 32 data-sets from the following experiments: BES at  $\sqrt{s} = 2\text{--}5$  GeV [23]; TASSO at  $\sqrt{s} = 14\text{--}44$  GeV [24, 25]; TPC at  $\sqrt{s} = 29$  GeV [26]; TOPAZ at  $\sqrt{s} = 58$  GeV [27]; ALEPH [28], L3 [29] and OPAL [6, 30] at  $\sqrt{s} = 91.2$  GeV; ALEPH [31, 34], DELPHI [32] and OPAL [33] at  $\sqrt{s} = 133$  GeV; and ALEPH [34] and OPAL [35–37] in the range  $\sqrt{s} = 161\text{--}202$  GeV. The total number of points is 1019 and the systematic and statistical uncertainties of the spectra are added in quadrature.

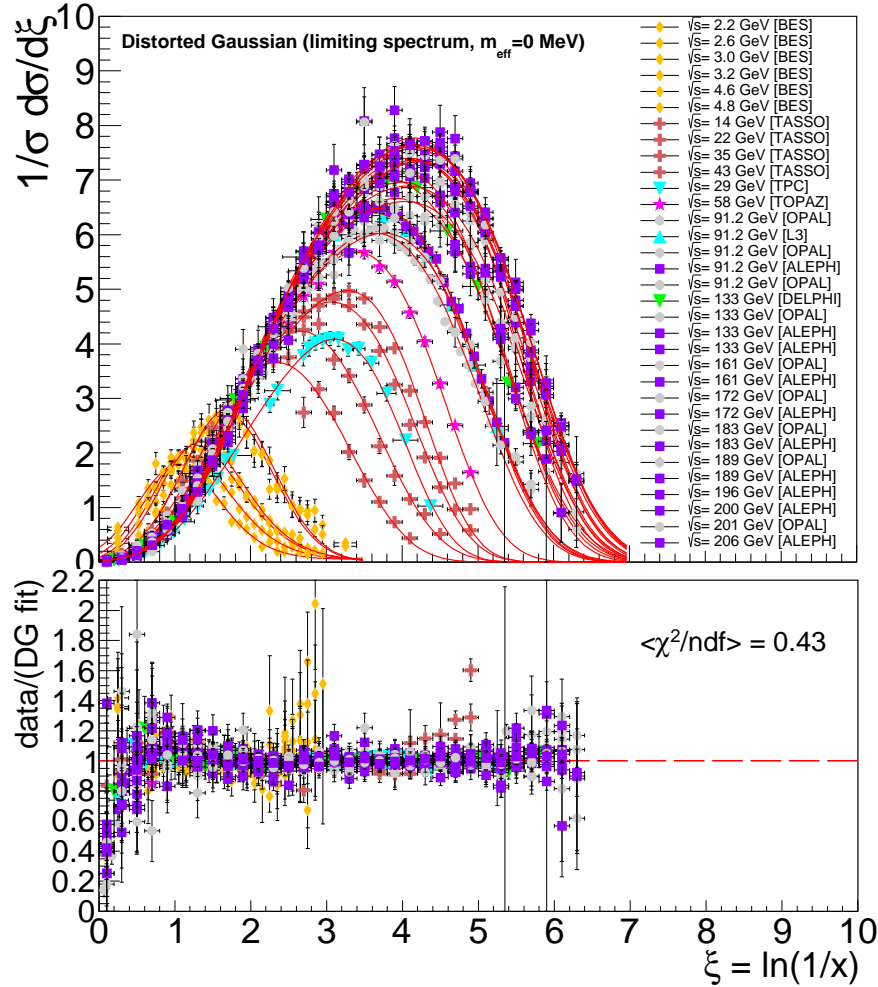


Figure 8: Top: Single inclusive hadron distributions measured in jets in the world  $e^+e^-$  data at  $\sqrt{s} \approx 2\text{--}200$  GeV as a function of  $\xi = \ln(\sqrt{s}/(2p_h))$  fitted to the distorted Gaussian Eq. (112) with  $m_{\text{eff}} = 0$ . Bottom: Ratio of each set of data points to the corresponding DG fit. The value  $\langle \chi^2/\text{ndf} \rangle$  quoted is the average of all individual fits.

In order to assess the effect of finite-mass corrections discussed in the previous Section, we carry out the DG fits of the data to Eq. (112) for many values of  $m_{\text{eff}}$  in the range 0–320 MeV. The lower value assumes that hadron and parton spectra are identical, the upper choice corresponds to an average of the pion, kaon and (anti)proton masses weighted by their corresponding abundances (65%, 30% and 5% approximately) in  $e^+e^-$  collisions. Representative fits of all the single-inclusive hadron distributions for  $m_{\text{eff}} = 0, 140$ , and 320 MeV are shown in Figures 8–10 respectively, with the norm, peak, width, skewness, and kurtosis as free parameters. In all cases the individual data-model agreement is very good,

with goodness-of-fit per degree-of-freedom  $\chi^2/\text{ndf} \approx 0.5\text{--}2.0$ , as indicated in the data/fit ratios around unity in the bottom panels. The fits to all datasets with energies above  $\sqrt{s} = 50$  GeV turn out to be completely insensitive to the choice of  $m_{\text{eff}}$ , i.e. the moments of the DG obtained are “invariant” with respect to the value of  $m_{\text{eff}}$ , whereas those at lower energies are more sensitive to it. The value of the effective mass that provides an overall best agreement to the whole set of experimental distributions is  $m_{\text{eff}} \approx 140$  MeV, which is consistent with a dominant pion composition of the inclusive charged hadron spectra.

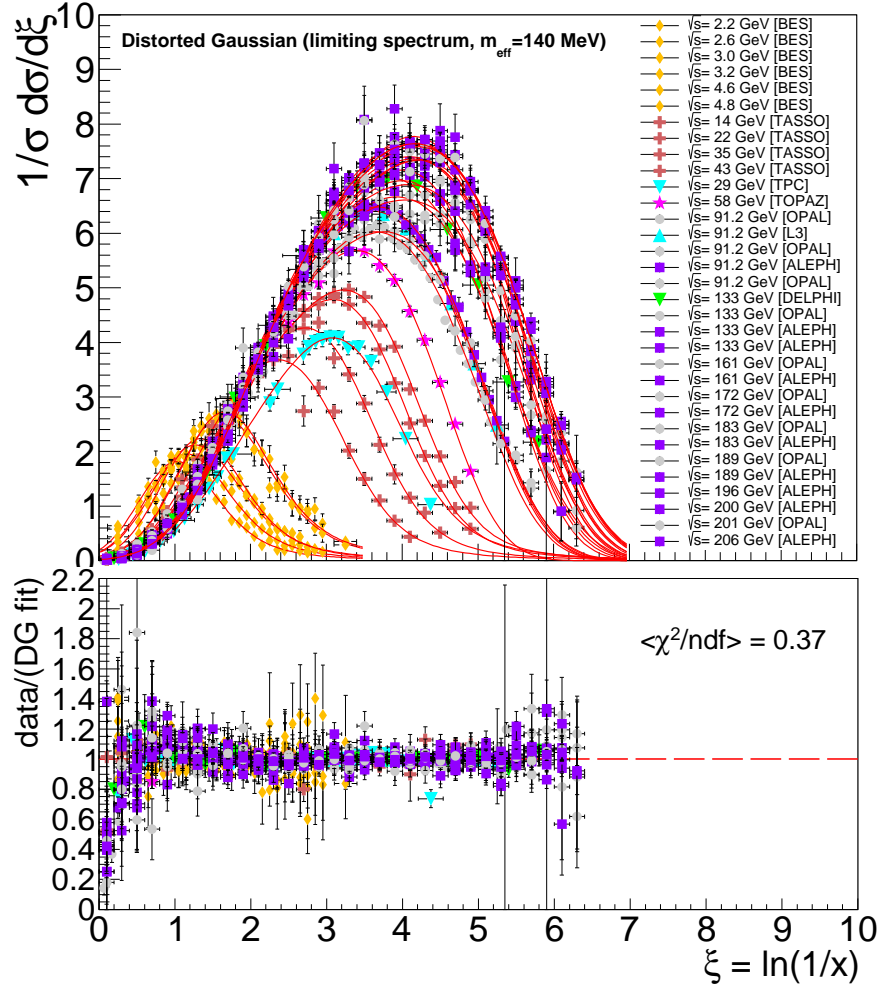


Figure 9: Top: Single inclusive hadron distributions measured in jets in the world  $e^+e^-$  data at  $\sqrt{s} \approx 2\text{--}200$  GeV as a function of  $\xi = \ln(\sqrt{s}/(2p_h))$  fitted to the distorted Gaussian Eq. (112) with  $m_{\text{eff}} = 140$  MeV Bottom: Ratio of each set of data points to the corresponding DG fit. The value  $\langle \chi^2/\text{ndf} \rangle$  quoted is the average of all individual fits.

The general trends of the DG moments are already visible in these plots: as  $\sqrt{s}$  increases, the peak of the distribution shifts to larger values of  $\xi$  (i.e. smaller relative values of the charged-hadron momenta) and the spectrum broadens (i.e. its width  $\sigma$  increases). In the range of the current measurements, the peak moves from  $\xi_{\text{max}} \approx 1$  to  $\xi_{\text{max}} \approx 4$ , and the width increases from  $\sigma \approx 0.5$  to 1.2. The expected logarithmic-like energy dependence of the peak of the  $\xi$  distribution, given by Eq. (102), due to soft gluon coherence (angular ordering), correctly reproduces the suppression of hadron production at small  $x$  seen

in the data to the right of the distorted Gaussian peak. Although a decrease at large  $\xi$  (very small  $x$ ) is expected based on purely kinematic arguments, the peak position would vary twice as rapidly with the energy in such a case in contradiction with the calculations and data. The integral of the  $\xi$  distribution gives the total charged-hadron multiplicity  $\mathcal{N}^{\text{ch}}$  which increases exponentially as per Eq. (100).

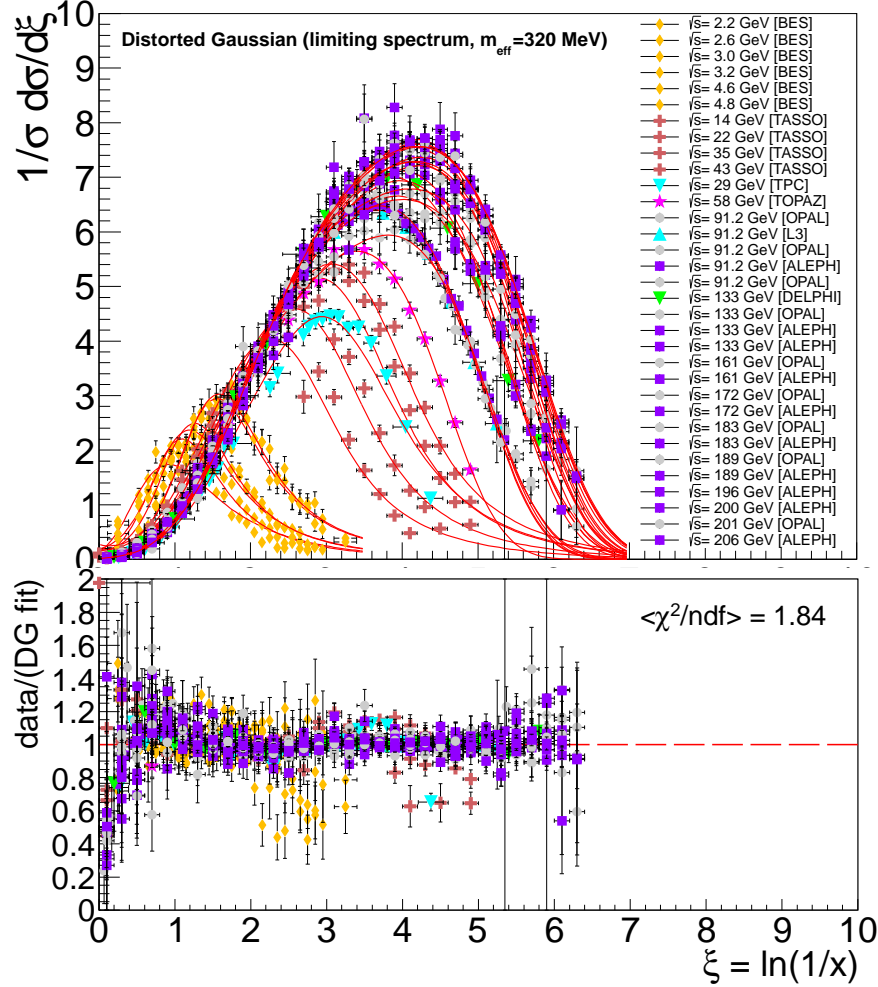


Figure 10: Top: Single inclusive hadron distributions measured in jets in the world  $e^+e^-$  data at  $\sqrt{s} \approx 2\text{--}200$  GeV as a function of  $\xi = \ln(\sqrt{s}/(2p_h))$  fitted to the distorted Gaussian Eq. (112) with  $m_{\text{eff}} = 320$  MeV. Bottom: Ratio of each set of data points to the corresponding DG fit. The value  $\langle \chi^2/\text{ndf} \rangle$  quoted is the average of all individual fits.

The  $\sqrt{s}$ -dependence of each one of the individual DG moments is studied by fitting their evolution to our NMLLA+NLO\* limiting-spectrum predictions Eqs. (100)–(105) with  $Y = \ln(\sqrt{s}/(2\Lambda_{\text{QCD}}))$  for  $n_f = 5$  quark flavours, with  $\Lambda_{\text{QCD}}$  as the only free parameter. Before performing the combined energy-dependence fit, the moments of the lowest- $\sqrt{s}$  distribution from the BES experiment are corrected to account for their different number of active flavours ( $n_f = 3, 4$ ) as described in the previous Section.

The collision-energy dependencies of all the obtained DG components are plotted in Figs. 11–15 for  $m_{\text{eff}} = 0.14$  GeV which, as aforementioned, provides the best individual fit to the DGs. In any case, using alternative  $m_{\text{eff}}$  values results only in small changes in the derived values of  $\Lambda_{\text{QCD}}$ , consistent with

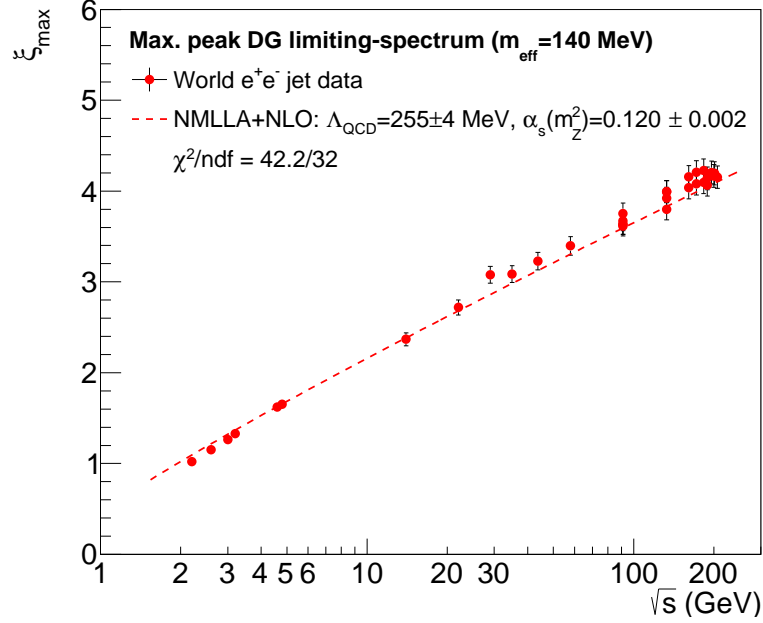


Figure 11: Energy evolution of the maximum peak position  $\xi_{\max}$  of the spectrum of charged hadrons in jets measured in  $e^+e^-$  at collision energies  $\sqrt{s} \approx 2\text{--}200$  GeV, fitted to Eq. (102) with  $Y = \ln(\sqrt{s}/(2\Lambda_{\text{QCD}}))$ , with finite-mass corrections ( $m_{\text{eff}} = 0.14$  GeV). The extracted values of  $\Lambda_{\text{QCD}}$  and equivalent  $\text{NLO}_{\overline{\text{MS}}} \alpha_s(m_Z^2)$  and the goodness-of-fit per degree-of-freedom  $\xi^2/\text{ndf}$ , are quoted.

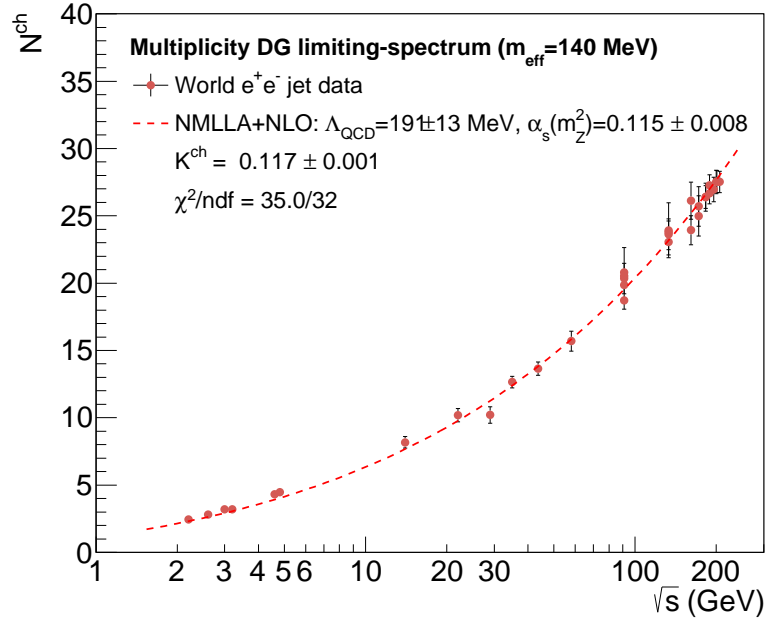


Figure 12: Energy evolution of the total multiplicity  $\mathcal{N}^{\text{ch}}$  spectrum of charged hadrons in jets measured in  $e^+e^-$  at collision energies  $\sqrt{s} \approx 2\text{--}200$  GeV, fitted to Eq. (100) with  $Y = \ln(\sqrt{s}/(2\Lambda_{\text{QCD}}))$ , with finite-mass corrections ( $m_{\text{eff}} = 0.14$  GeV). The extracted values of the  $\mathcal{K}^{\text{ch}}$  normalization constant,  $\Lambda_{\text{QCD}}$  and equivalent  $\text{NLO}_{\overline{\text{MS}}} \alpha_s(m_Z^2)$ , and the goodness-of-fit per degree-of-freedom  $\xi^2/\text{ndf}$ , are quoted.

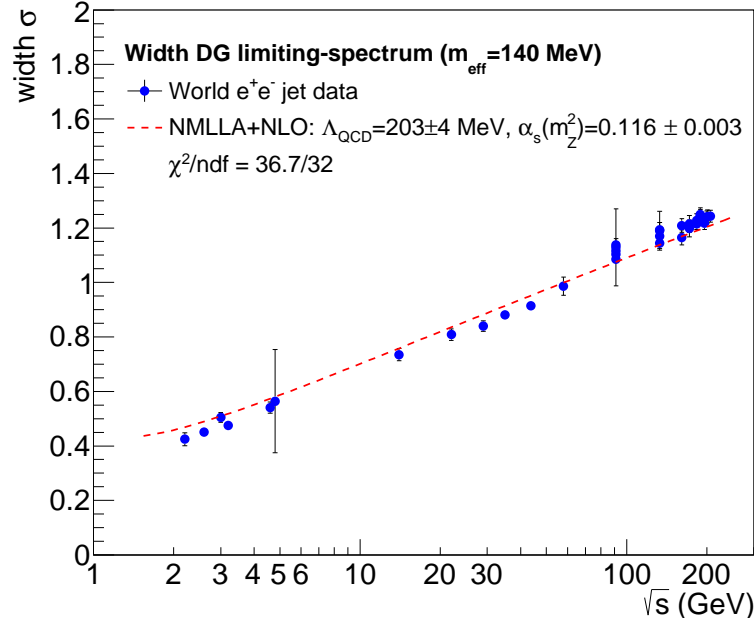


Figure 13: Energy evolution of the width  $\sigma$  spectrum of charged hadrons in jets measured in  $e^+e^-$  at collision energies  $\sqrt{s} \approx 2\text{--}200$  GeV, fitted to Eq. (103) with  $Y = \ln(\sqrt{s}/(2\Lambda_{\text{QCD}}))$ , with finite-mass corrections ( $m_{\text{eff}} = 0.14$  GeV). The extracted values of  $\Lambda_{\text{QCD}}$  and equivalent NLO $_{\overline{\text{MS}}}$   $\alpha_s(m_Z^2)$ , and the goodness-of-fit per degree-of-freedom  $\chi^2/\text{ndf}$ , are quoted.

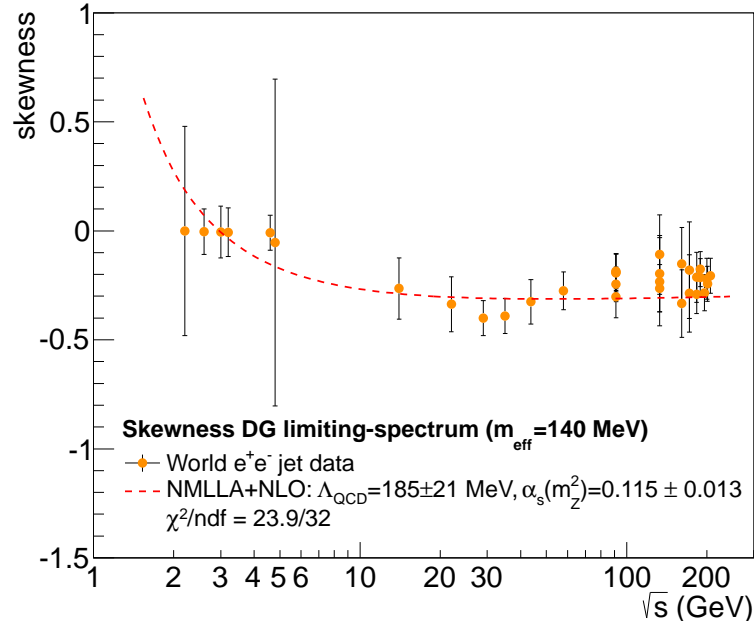


Figure 14: Energy evolution of the skewness  $s$  of the spectrum of charged hadrons in jets measured in  $e^+e^-$  at collision energies  $\sqrt{s} \approx 2\text{--}200$  GeV, fitted to Eq. (104) with  $Y = \ln(\sqrt{s}/(2\Lambda_{\text{QCD}}))$ , with finite-mass corrections ( $m_{\text{eff}} = 0.14$  GeV). The extracted values of  $\Lambda_{\text{QCD}}$  and equivalent NLO $_{\overline{\text{MS}}}$   $\alpha_s(m_Z^2)$ , and the goodness-of-fit per degree-of-freedom  $\chi^2/\text{ndf}$ , are quoted.

its quoted uncertainties. Varying  $m_{\text{eff}}$  from zero to 0.32 GeV yields differences in the extracted  $\Lambda_{\text{QCD}}$  parameter below  $\pm 0.5\%$  for the  $\xi_{\text{max}}$  fits and below  $\pm 2\%$  for the other components, which indicate the robustness of our NMLLA+NLO\* calculations for the limiting-spectrum DG with respect to finite-mass effects if a wide enough range of charged-hadron and parent-parton (jet) energies are considered in the evolution fit. The point-to-point uncertainties of the different moments, originally coming from the DG fit procedure alone, have been enlarged so that their minimum values are at least 3% for the peak position, and 5% for the multiplicity and width. Such minimum uncertainties are consistent with the spread of the DG moments obtained for different experiments at the same collision-energies, and guarantee an acceptable global goodness-of-fit  $\chi^2/\text{ndf} \approx 1$  for their  $\sqrt{s}$ -dependence. We note that not all measurements originally corrected for feed-down contributions from weak decays of primary particles. This affects, in particular, the multiplicities measured for the TASSO [24, 25], TPC [26] and OPAL [6] datasets which include charged particles from  $K_0^0$  and  $\Lambda$  decays. The effect on the peak position (and higher HBP moments) of including secondary particles from decays is negligible ( $< 0.5\%$ ), but increases the total charged particles yields by 8% according to experimental data and Monte Carlo simulations [45]. For these three data-sets, we have thus reduced accordingly the value of  $\mathcal{N}^{\text{ch}}$ .

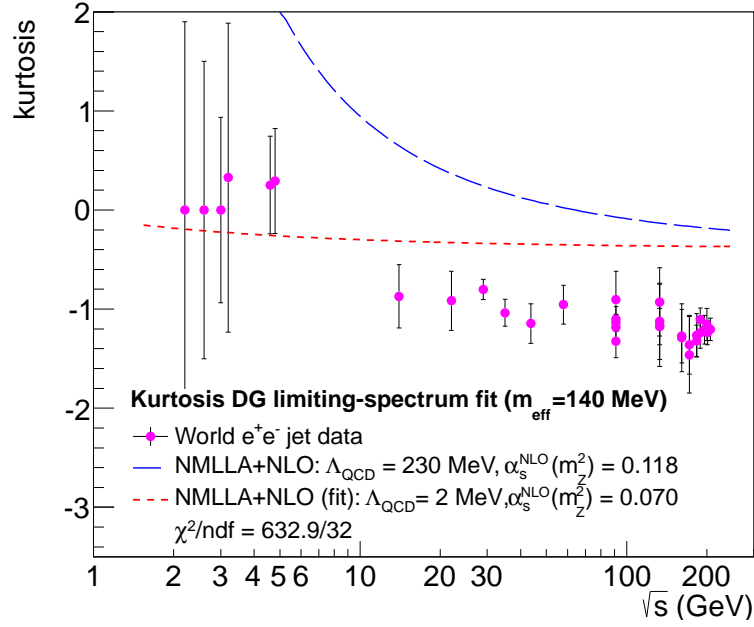


Figure 15: Energy evolution of the kurtosis  $k$  of the spectrum of charged hadrons in jets measured in  $e^+e^-$  at collision energies  $\sqrt{s} \approx 2\text{--}200$  GeV, fitted to Eq. (105) with  $Y = \ln(\sqrt{s}/(2\Lambda_{\text{QCD}}))$ , with finite-mass corrections ( $m_{\text{eff}} = 0.14$  GeV). The resulting  $\Lambda_{\text{QCD}}$ ,  $\text{NLO}_{\overline{\text{MS}}} \alpha_s(m_Z^2)$ , and goodness-of-fit per degree-of-freedom  $\chi^2/\text{ndf}$  are quoted. The long-dashed curve shows the expected theoretical dependence for  $\Lambda_{\text{QCD}} = 230$  MeV.

The DG skewness and kurtosis are less well constrained by the individual fits to the measured fragmentation functions and have much larger uncertainties than the rest of moments. As a matter of fact, in the case of the kurtosis our NMLLA+NLO\* prediction for its energy-evolution Eq. (105), fails to provide a proper description of the data and seems to be above the data by a constant offset (Fig. 15). Whether this fact is due to missing higher-order contributions in our calculations or to other effects is not yet clear at this point. Apart from the kurtosis, the QCD coupling value extracted from all the other moments has



values around  $\alpha_s(m_Z^2) = 0.118$ , in striking agreement with the current world-average obtained by other methods [56,57].

Table 1: Values of  $\Lambda_{\text{QCD}}$  and associated  $\alpha_s(m_Z^2)$  at NLO ( $\overline{\text{MS}}$  scheme,  $n_f = 5$  quark flavours) obtained from the fits of the  $\sqrt{s}$ -dependence of the moments of the charged hadron distribution of jets in  $e^+e^-$  collisions obtained from their NMLLA+NLO\* evolution. The last column provides the weighted-average of the individual measurements with its total propagated uncertainty.

DG moment:	Peak position	Multiplicity	Width	Skewness	Combined
$\Lambda_{\text{QCD}}$ (MeV)	$255 \pm 4$	$191 \pm 13$	$203 \pm 4$	$185 \pm 21$	$249 \pm 6$
$\alpha_s(m_Z^2)$	$0.120 \pm 0.002$	$0.115 \pm 0.008$	$0.116 \pm 0.003$	$0.115 \pm 0.013$	$0.1195 \pm 0.0022$

Table 1 lists each value of the  $\Lambda_{\text{QCD}}$  parameter individually extracted from the energy evolutions of the four DG components that are well described by our NMLLA+NLO\* approach, and their associated values of  $\alpha_s(m_Z^2)$  obtained using the two-loop Eq. (9) for  $n_f = 5$  quark flavours. Whereas the errors quoted for the different  $\Lambda_{\text{QCD}}$  values include only uncertainties from the fit procedure, the propagated  $\alpha_s(m_Z^2)$  uncertainties have been enlarged by a common factor such that their final weighted average has a  $\chi^2/\text{ndf}$  close to unity. Such a “ $\chi^2$  averaging” method [57] takes into account in a well defined manner any correlations between the four extractions of  $\alpha_s$ , as well as underestimated systematic uncertainties. The relative uncertainty of the  $\alpha_s(m_Z^2)$  determination from the DG moments evolution is about  $\pm 1.5\%$  for the maximum peak position,  $\pm 3.5\%$  for the width,  $\pm 7\%$  for the total multiplicity, and about  $\pm 11\%$  for the skewness. The last column of Table 1 lists the final values of  $\Lambda_{\text{QCD}}$  and  $\alpha_s(m_Z^2)$  determined by taking the weighted-average of the four individual measurements. We obtain a final value  $\alpha_s(m_Z^2) = 0.1195 \pm 0.0022$  which is in excellent agreement with the current world-average of the strong coupling at the Z mass [56,57]. Our extraction of the QCD strong coupling has an uncertainty ( $\pm 2\%$ ) that is commensurate with that from other  $e^+e^-$  observables such as jet-shapes ( $\pm 1\%$ ) and 3-jets rates ( $\pm 2\%$ ) [56,57]. In a forthcoming work, we extend the extraction of the strong coupling via the NMLLA+NLO\* evolution of the moments of the hadron distribution in jet world-data measured not only in  $e^+e^-$  but also including deep-inelastic  $e^\pm p$  collisions [58].

## 5 Conclusions and outlook

We have computed analytically the energy evolution of the moments of the single-inclusive distribution of hadrons inside QCD jets in the next-to-modified-leading-log approximation (NMLLA) including next-to-leading-order (NLO) corrections to the  $\alpha_s$  strong coupling. Using a distorted Gaussian parametrization, we provide in a closed-form the numerical expressions for the energy-dependence of the maximum peak position, total multiplicity, peak width, kurtosis and skewness of the limiting spectra where the hadron distributions are evolved down to the  $\Lambda_{\text{QCD}}$  scale. Comparisons of all the existing jet data measured in  $e^+e^-$  collisions in the range  $\sqrt{s} \approx 2\text{--}200$  GeV to the NMLLA+NLO\* predictions for the moments of the hadron distributions allow one to extract a value of the QCD parameter  $\Lambda_{\text{QCD}}$  and associated two-loop coupling constant at the Z resonance,  $\alpha_s(m_Z^2) = 0.1195 \pm 0.0022$ , in excellent agreement with the current world average obtained with other methods. The NMLLA+NLO\* approach presented here can be further extended to full NMLLA+NLO through the inclusion of the two-loop splitting functions. Also, in a forthcoming phenomenological study we plan to compare our approach not only to the world  $e^+e^-$  jet

data but also to jet measurements in (the current hemisphere of the Breit-frame of) deep-inelastic  $e^\pm p$  collisions. The application of our approach to the hadron distribution of TeV-jets produced in proton-proton collisions at LHC energies would further allow one to extract  $\alpha_s$  from parton-to-hadron FFs over a very wide kinematic range. The methodology presented here provides a new independent approach for the determination of the QCD coupling constant complementary to other existing jet-based methods –relying on jet shapes, and/or on ratios of N-jet production cross sections– with a totally different set of experimental and theoretical uncertainties.

## Acknowledgments

We are grateful to Yuri Dokshitzer, Igor Dremin, Kari Eskola, Valery A. Khoze, Sven Moch, Wolfgang Ochs, and Bryan Webber for useful discussions and/or comments to a previous version of this manuscript. R. Pérez-Ramos acknowledges support from the Academy of Finland, Projects No. 130472 and No.133005.

## Appendix

### A Mellin-transformed splitting functions

The set of LO DGLAP splitting functions in Mellin space has been given in [46]. It follows from Eqs. (7)–(8) by making use of the Mellin transform given in Eq. (19) such that

$$P_{gg}(\Omega) = -4N_c [\psi(\Omega + 1) + \gamma_E] + \frac{11N_c}{3} - \frac{2n_f}{3} + \frac{8N_c(\Omega^2 + \Omega + 1)}{\Omega(\Omega^2 - 1)(\Omega + 2)}, \quad (114a)$$

$$P_{gq}(\Omega) = \frac{\Omega^2 + \Omega + 2}{\Omega(\Omega + 1)(\Omega + 2)}, \quad (114b)$$

$$P_{qg}(\Omega) = 2C_F \frac{\Omega^2 + \Omega + 2}{\Omega(\Omega^2 - 1)}, \quad (114c)$$

$$P_{qq}(\Omega) = -C_F \left[ \psi(\Omega + 1) + 4\gamma_E - 3 - \frac{2}{\Omega(\Omega + 1)} \right]. \quad (114d)$$

The expansion of the set of splitting functions (114a)–(114d) in Mellin space is trivial and makes use of the Taylor expansion of the digamma function as  $\Omega \rightarrow 0$ :

$$\psi(\Omega + 1) = -\gamma_E + \frac{\pi^2}{6}\Omega + \mathcal{O}(\Omega^2),$$

and  $(1 \pm \Omega)^\alpha \approx 1 \mp \alpha\Omega + \frac{1}{2}\alpha(\alpha - 1)\Omega^2 + \dots$ , which leads to the formulæ (20a)–(20d).

## B NMLLA+NLO\* moments $K_n$ of the distorted Gaussian

We compute here the generic for the moments of the distorted Gaussian (DG) for  $\lambda \neq 0$  according to Eq. (38) by introducing the following functions:

$$f_1(Y, \lambda) = \frac{1 - \frac{\lambda}{Y+\lambda}}{1 - \left(\frac{\lambda}{Y+\lambda}\right)^{3/2}}, \quad f_4(Y, \lambda) = \frac{1 - \left(\frac{\lambda}{Y+\lambda}\right)^2}{1 - \left(\frac{\lambda}{Y+\lambda}\right)^{5/2}} \quad (115)$$

$$f_2(Y, \lambda) = \frac{1 - \left(\frac{\lambda}{Y+\lambda}\right)^{1/2}}{1 - \left(\frac{\lambda}{Y+\lambda}\right)^{3/2}}, \quad f_5(Y, \lambda) = \frac{1 - \left(\frac{\lambda}{Y+\lambda}\right)^{3/2}}{1 - \left(\frac{\lambda}{Y+\lambda}\right)^{5/2}}, \quad (116)$$

$$f_3(Y, \lambda) = \frac{1 - \left(\frac{\lambda}{Y+\lambda}\right)^{1/2} \left[ \frac{\ln 2\lambda - 2}{\ln 2(Y+\lambda) - 2} \right]}{1 - \left(\frac{\lambda}{Y+\lambda}\right)^{3/2}}, \quad f_6(Y, \lambda) = \frac{1 - \left(\frac{\lambda}{Y+\lambda}\right)^{3/2} \left[ \frac{\ln 2\lambda - 2/3}{\ln 2(Y+\lambda) - 2/3} \right]}{1 - \left(\frac{\lambda}{Y+\lambda}\right)^{5/2}}. \quad (117)$$

Notice that  $f_i(Y, \lambda = 0) = 1$ . The expressions for  $K_2$ ,  $K_3$ ,  $K_4$  and  $K_5$  are then, respectively:

$$K_2(Y, \lambda) = \frac{Y + \lambda}{3} \sqrt{\frac{\beta_0(Y + \lambda)}{16N_c}} \left[ 1 - \left(\frac{\lambda}{Y + \lambda}\right)^{3/2} \right] \left\{ 1 - \frac{1}{32} \beta_0 f_1(Y, \lambda) \sqrt{\frac{16N_c}{\beta_0(Y + \lambda)}} \right. \\ \left. + \left[ \frac{9}{8} a_2 f_2(Y, \lambda) - \frac{3}{32} \left( \frac{3}{16N_c^2} a_1^2 + \frac{a_1 \beta_0}{8N_c^2} - \frac{\beta_0^2}{64N_c^2} \right) f_2(Y, \lambda) \right. \right. \\ \left. \left. + \frac{\beta_1}{32\beta_0} (\ln 2(Y + \lambda) - 2) f_3(Y, \lambda) \right] \frac{16N_c}{\beta_0(Y + \lambda)} \right\} \quad (118)$$

$$K_3(Y, \lambda) = -\frac{a_1}{64N_c} \sqrt{\frac{\beta_0}{N_c}} (Y + \lambda)^{3/2} \left[ 1 - \left(\frac{\lambda}{Y + \lambda}\right)^{3/2} \right] \left( 1 - \frac{\beta_0}{16} f_1(Y, \lambda) \sqrt{\frac{16N_c}{\beta_0(Y + \lambda)}} \right) \quad (119)$$

$$K_4(Y, \lambda) = -\frac{3}{320} \left(\frac{\beta_0}{N_c}\right)^{3/2} (Y + \lambda)^{5/2} \left[ 1 - \left(\frac{\lambda}{Y + \lambda}\right)^{5/2} \right] \left\{ 1 - \frac{5}{48} \beta_0 f_4(Y, \lambda) \sqrt{\frac{16N_c}{\beta_0(Y + \lambda)}} \right. \\ \left. + \left[ \frac{25}{24} a_2 f_5(Y, \lambda) - \frac{5}{256} \left( \frac{5}{2N_c^2} a_1^2 + \frac{a_1 \beta_0}{N_c^2} - \frac{55}{24N_c^2} \beta_0^2 \right) f_5(Y, \lambda) \right. \right. \\ \left. \left. + \frac{5\beta_1}{96\beta_0} \left( \ln 2(Y + \lambda) - \frac{2}{3} \right) f_6(Y, \lambda) \right] \frac{16N_c}{\beta_0(Y + \lambda)} \right\} \quad (120)$$

$$K_5(Y, \lambda) = \frac{3a_1\beta_0^2(Y + \lambda)^2}{4096N_c^3} \left( 10 + 12 \sqrt{\frac{N_c(Y + \lambda)}{\beta_0}} \right) - \frac{3a_1\beta_0^2\lambda^2}{4096N_c^3} \left( 10 + 12 \sqrt{\frac{N_c\lambda}{\beta_0}} \right). \quad (121)$$

Compared to MLLA, a new term appears in the expression (119) of  $K_3$ . In order to determine the dispersion  $\sigma$ , the skewness  $s$  and kurtosis of the distribution, we need to normalise by the corresponding power of  $\sigma$ . After taking the  $\sigma = \sqrt{K_2}$  and expanding the Taylor series in  $1/\sqrt{Y}$ , we find the following expressions:

$$\sigma^{-3}(Y, \lambda) = \left(\frac{3}{Y + \lambda}\right)^{3/2} \left(\frac{16N_c}{\beta_0(Y + \lambda)}\right)^{3/4} \left[ 1 - \left(\frac{\lambda}{Y + \lambda}\right)^{3/2} \right]^{-3/2} (1$$

$$+ \frac{3\beta_0}{64} f_1(Y, \lambda) \sqrt{\frac{16N_c}{\beta_0(Y + \lambda)}}, \quad (122)$$

$$\begin{aligned} \sigma^{-4}(Y, \lambda) = & \left( \frac{3}{Y + \lambda} \right)^2 \frac{16N_c}{\beta_0(Y + \lambda)} \left[ 1 - \left( \frac{\lambda}{Y + \lambda} \right)^{3/2} \right]^{-2} \left\{ 1 + \frac{\beta_0}{16} f_1(Y, \lambda) \sqrt{\frac{16N_c}{\beta_0(Y + \lambda)}} \right. \\ & - \left[ \frac{9}{4} a_2 f_2(Y, \lambda) - \frac{3}{16} \left( \frac{3a_1^2}{16N_c^2} f_2(Y, \lambda) + \frac{a_1\beta_0}{8N_c^2} f_2(Y, \lambda) - \frac{\beta_0^2}{64N_c^2} f_2(Y, \lambda) \right) \right. \\ & \left. \left. + \frac{9\beta_0^2}{64N_c^2} f_1^2(Y, \lambda) \right) + \frac{\beta_1}{16\beta_0} (\ln 2(Y + \lambda) - 2) f_3(Y, \lambda) \right] \frac{16N_c}{\beta_0(Y + \lambda)} \left. \right\}, \quad (123) \end{aligned}$$

$$\begin{aligned} \sigma^{-5}(Y) = & \left( \frac{3}{Y + \lambda} \right)^{5/2} \left( \frac{16N_c}{\beta_0(Y + \lambda)} \right)^{5/4} \left[ 1 - \left( \frac{\lambda}{Y + \lambda} \right)^{3/2} \right]^{-5/2} (1 \\ & + \frac{5\beta_0}{64} f_1(Y, \lambda) \sqrt{\frac{16N_c}{\beta_0(Y + \lambda)}}). \quad (124) \end{aligned}$$

Thus  $\sigma^{-3}$ ,  $\sigma^{-4}$  and  $\sigma^{-5}$  expressions should be multiplied by  $K_3$ ,  $K_4$  and  $K_5$  and the result re-expanded again in order to get the final results of Eqs. (50), (52) and (45) respectively.

## C Higher-order corrections to the moments of the distorted Gaussian

We extract here some corrections to be incorporated into the perturbative expansion of the truncated series for the mean peak position, dispersion, skewness and kurtosis [52]. The presence of these corrections in the exact solution of the MLLA evolution equations is far from trivial and is thus detailed in this appendix. These corrections are indeed hidden in the exact solution of the MLLA evolution equations with one-loop coupling constant and can be extracted after performing some algebraical calculations as described in [52] (see also [4] and references therein). The exact solution was written in terms of confluent hypergeometric functions and then in terms of fast convergent Bessel series as follows [4]:

$$\mathcal{D}^+(\xi, Y) = \frac{8N_c \Gamma(B)}{\beta_0} \int_0^{\frac{\pi}{2}} \frac{d\tau}{\pi} e^{-B\alpha} \mathcal{F}_B(\tau, Y, \xi), \quad (125)$$

where the integration is performed with respect to  $\tau$  defined by  $\alpha = \frac{1}{2} \ln \frac{Y - \xi}{\xi} + i\tau$  and with

$$\begin{aligned} \mathcal{F}_B(\tau, Y, \xi) &= \left[ \frac{\cosh \alpha - \frac{Y - 2\xi}{Y} \sinh \alpha}{\frac{4N_c Y}{\beta_0} \frac{\alpha}{\sinh \alpha}} \right]^{B/2} I_B(2\sqrt{Z(\tau, Y, \xi)}), \\ Z(\tau, Y, \xi) &= \frac{4N_c Y}{\beta_0} \frac{\alpha}{\sinh \alpha} \left( \cosh \alpha - \frac{Y - 2\xi}{Y} \sinh \alpha \right), \end{aligned}$$

$B = a_1/\beta_0$  and  $I_B$  is the modified Bessel function of the first kind. It was then possible to extract the moments of the DG from this more complicated approach also. In the end, the MLLA moments of the DG found in [22] from the MLLA anomalous dimension allows one to cross check the MLLA expressions found in [4]. According to [52],

$$\xi_n = Y^n \cdot \mathcal{L}_n(B + 1, B + 2, z), \quad B = \frac{a_1}{\beta_0}, \quad z = \sqrt{\frac{16N_c}{\beta_0}} Y, \quad (126)$$

where the function  $\mathcal{L}_n$  was written in the form of the series,

$$\mathcal{L}_n(B+1, B+2; z) = P_0^{(n)}(B+1, B+2; z) + \frac{2 I_{B+2}(z)}{z I_{B+1}(z)} \cdot P_1^{(n)}(B+1, B+2; z),$$

with

$$P_0^{(n)}(B+1, B+2; z) = \sum_{k=0}^{n-1} \alpha_{n-k}^{(n)} \left(\frac{2}{z}\right)^{2k}, \quad P_1^{(n)}(B+1, B+2; z) = \sum_{k=0}^{n-1} \beta_{n-k}^{(n)} \left(\frac{2}{z}\right)^{2k}. \quad (127)$$

The functions  $I_{B+i}(z)$  correspond to the modified Bessel series of the second kind. The leading coefficients are defined as:

$$\alpha_n^{(n)} = 2^{-n}, \quad \beta_n^{(n)} = \frac{n}{2^n} \left(B + \frac{n-1}{3}\right)$$

and the others  $\alpha_{n-k}^{(n)}, \beta_{n-k}^{(n)}$  for  $k \neq 0$  are the solutions of the triangular matrix

$$\begin{pmatrix} 1 & 0 & 0 & 0 & 0 & 0 \\ 1 & B+2 & 0 & 0 & 0 & 0 \\ 1 & 1 & -B-1 & 0 & 0 & 0 \\ 1 & B+3 & B+3 & (B+2)(B+3) & 0 & 0 \\ 1 & 2 & -2B & -2B & 2B(B+1) & 0 \\ 1 & B+3 & B+4 & (B+3)(B+4) & (B+3)(B+4) & (B+2)(B+3)(B+4) \end{pmatrix} \begin{pmatrix} \beta_1^{(n)} \\ \alpha_1^{(n)} \\ \beta_2^{(n)} \\ \alpha_2^{(n)} \\ \beta_3^{(n)} \\ \alpha_3^{(n)} \end{pmatrix} = \begin{pmatrix} -\frac{\Phi_{-B-1}^{(n)}}{B+1} \\ 0 \\ -\frac{\Phi_{-B}^{(n)}}{B} \\ 0 \\ -\frac{\Phi_{-B+1}^{(n)}}{B-1} \\ 0 \end{pmatrix}. \quad (128)$$

The functions  $\Phi$  in the r.h.s. of Eq. (128) are defined in the form

$$\Phi_c^{(1)} = \frac{1}{2} \{c\}_2 + (B+1) \{c\}_1, \quad (129)$$

$$\Phi_c^{(2)} = \frac{1}{4} \{c\}_4 + \left(B + \frac{5}{3}\right) \{c\}_3 + (B+1)(B+2) \{c\}_2, \quad (130)$$

$$\begin{aligned} \Phi_c^{(3)} &= \frac{1}{8} \{c\}_6 + \frac{1}{4} (3B+7) \{c\}_5 + \frac{1}{2} (3B^2 + 13B + 13) \{c\}_4 \\ &+ (B+1)(B+2)(B+3) \{c\}_3, \end{aligned} \quad (131)$$

$$\begin{aligned} \Phi_c^{(4)} &= \frac{1}{16} \{c\}_8 + \frac{1}{2} (B+3) \{c\}_7 + \left(\frac{3}{2} B^2 + \frac{17}{2} B + \frac{34}{3}\right) \{c\}_6 \\ &+ \left[2(B+1)^3 + 10(B+1)^2 + 14(B+1) + \frac{24}{5}\right] \{c\}_5 \\ &+ (B+1)(B+2)(B+3)(B+4) \{c\}_4, \end{aligned} \quad (132)$$

where the shorthand notation  $\{c\}_p = c(c-1) \dots (c-p+1)$  has been introduced for the sake of simplicity and  $c = -B-1, -B, -B+1$  according to the r.h.s. of Eq. (128). For instance, making use of Eq. (74), for  $n = 1$  one has,

$$\xi_1 = Y \cdot \mathcal{L}(B+1, B+2; z) = Y \left[ P_0^{(1)}(B+1, B+2; z) + \frac{2 I_{B+2}(z)}{z I_{B+1}(z)} \cdot P_1^{(1)}(B+1, B+2; z) \right],$$

where in this case:

$$P_0^{(1)}(B+1, B+2; z) = \alpha_1^{(1)} = \frac{1}{2}, \quad P_1^{(1)}(B+1, B+2; z) = \beta_1^{(1)} = \frac{1}{2}B,$$

according to the recursive relations given above. Therefore,

$$\xi_1 = \frac{Y}{2} \left[ 1 + \frac{2}{z} B \frac{I_{B+2}(z)}{I_{B+1}(z)} \right]. \quad (133)$$

Expanding the ratio  $I_{B+2}(z)/I_{B+1}(z)$  for large  $z$  (large energy scale in  $Y(E)$ ) and making use of the asymptotic expansion for the Bessel functions,

$$\begin{aligned} I_\nu(z) \approx & \frac{e^z}{\sqrt{2\pi z}} \left[ 1 - \frac{1}{2z} \left( \nu^2 - \frac{1}{4} \right) + \frac{1}{8z^2} \left( \nu^2 - \frac{9}{4} \right) \left( \nu^2 - \frac{1}{4} \right) \right. \\ & \left. - \frac{1}{48z^3} \left( \nu^2 - \frac{25}{4} \right) \left( \nu^2 - \frac{9}{4} \right) \left( \nu^2 - \frac{1}{4} \right) \right], \end{aligned} \quad (134)$$

one has

$$\frac{I_{B+2}(z)}{I_{B+1}(z)} = 1 - \frac{2B+3}{2z} + \frac{(2B+3)(2B+1)}{8z^2} + \frac{(2B+3)(2B+1)}{8z^3} + \mathcal{O}(z^{-4}). \quad (135)$$

## References

- [1] Y.L. Dokshitzer, V.S. Fadin and V.A. Khoze, Z. Phys. C18 (1983) 37.
- [2] Y.I. Azimov et al., Z. Phys. C27 (1985) 65.
- [3] B. Ermolaev and V.S. Fadin, JETP Lett. 33 (1981) 269.
- [4] Y.L. Dokshitzer et al., Gif-sur-Yvette, France: Ed. Frontières (1991) 274 p. (Basics of); and Rev. Mod. Phys. **60** (1988) 373.
- [5] Y.I. Azimov et al., Zeit. Phys. C31 (1986) 213.
- [6] OPAL Collaboration, M. Akrawy et al., Phys.Lett. B247 (1990) 617.
- [7] CDF Collaboration, T. Aaltonen et al., Phys. Rev. D77 (2008) 092001, arXiv:0802.3182.
- [8] Y.L. Dokshitzer, V.S. Fadin and V.A. Khoze, Zeit. Phys. C15 (1982) 325.
- [9] V.S. Fadin, Yad. Fiz. 37 (1983) 408.
- [10] V.A. Khoze and W. Ochs, Int. J. Mod. Phys. A12 (1997) 2949, hep-ph/9701421.
- [11] R. Pérez Ramos, F. Arleo and B. Machet, Phys. Rev. D78 (2008) 014019, 0712.2212.
- [12] F. Arleo, R. Pérez Ramos and B. Machet, Phys. Rev. Lett. 100 (2008) 052002, 0707.3391.
- [13] V.N. Gribov and L.N. Lipatov, Sov. J. Nucl. Phys. 15 (1972) 438.
- [14] G. Altarelli and G. Parisi, Nucl. Phys. B126 (1977) 298.
- [15] Y.L. Dokshitzer, Sov. Phys. JETP 46 (1977) 641.
- [16] Y.L. Dokshitzer, V.A. Khoze and S. Troian, Z.Phys. C55 (1992) 107.
- [17] A. Capella et al., Phys. Rev. D61 (2000) 074009, hep-ph/9910226.
- [18] F. Cuypers and K. Tesima, Z. Phys. C54 (1992) 87.
- [19] W.E. Caswell, Phys.Rev.Lett. 33 (1974) 244.
- [20] I.M. Dremin and J.W. Gary, Phys. Rept. 349 (2001) 301, hep-ph/0004215.
- [21] P. Bolzoni, B.A. Kniehl and A.V. Kotikov, (2013), 1305.6017.
- [22] C.P. Fong and B.R. Webber, Nucl. Phys. B355 (1991) 54.
- [23] BES Collaboration, W. Dunwoodie et al., Phys.Rev. D69 (2004) 072002, hep-ex/0306055.
- [24] TASSO Collaboration, W. Braunschweig et al., Z. Phys. C41 (1988) 359.
- [25] TASSO Collaboration, W. Braunschweig et al., Z. Phys. C47 (1990) 187.
- [26] TPC/Two Gamma Collaboration, H. Aihara et al., Phys. Rev. Lett. 61 (1988) 1263.
- [27] TOPAZ Collaboration, R. Itoh et al., Phys.Lett. B345 (1995) 335, hep-ex/9412015.

- [28] ALEPH Collaboration, R. Barate et al., Phys.Rept. 294 (1998) 1.
- [29] L3 Collaboration, B. Adeva et al., Phys. Lett. B259 (1991) 199.
- [30] OPAL Collaboration, K. Ackerstaff et al., Eur. Phys. J. C7 (1999) 369, hep-ex/9807004.
- [31] ALEPH Collaboration, D. Buskulic et al., Z. Phys. C73 (1997) 409.
- [32] DELPHI Collaboration, P. Abreu et al., Z. Phys. C73 (1997) 229.
- [33] OPAL Collaboration, G. Alexander et al., Z. Phys. C72 (1996) 191.
- [34] ALEPH Collaboration, A. Heister et al., Eur. Phys. J. C35 (2004) 457.
- [35] OPAL Collaboration, K. Ackerstaff et al., Z. Phys. C75 (1997) 193.
- [36] OPAL Collaboration, G. Abbiendi et al., Eur. Phys. J. C16 (2000) 185, hep-ex/0002012.
- [37] OPAL Collaboration, G. Abbiendi et al., Eur. Phys. J. C27 (2003) 467, hep-ex/0209048.
- [38] G. Altarelli et al., Nucl. Phys. B160 (1979) 301.
- [39] W. Furmanski and R. Petronzio, Zeit. Phys. C11 (1982) 293.
- [40] G. Curci, W. Furmanski and R. Petronzio, Nucl. Phys. B175 (1980) 27.
- [41] S. Albino et al., Eur. Phys. J. C36 (2004) 49, hep-ph/0404287.
- [42] S. Albino, B. Kniehl and G. Kramer, Eur. Phys. J. C38 (2004) 177, hep-ph/0408112.
- [43] S. Albino et al., Phys. Rev. Lett. 95 (2005) 232002, hep-ph/0503170.
- [44] S. Albino et al., Phys. Rev. D73 (2006) 054020, hep-ph/0510319.
- [45] T. Sjostrand, S. Mrenna and P. Skands, JHEP 05 (2006) 026, hep-ph/0603175.
- [46] Y.L. Dokshitzer, D. Diakonov and S.I. Troian, Phys. Rept. 58 (1980) 269.
- [47] A. Vogt, JHEP 1110 (2011) 025, 1108.2993.
- [48] Y.L. Dokshitzer et al., Phys.Lett. B273 (1991) 319.
- [49] I. Dremin and V. Nechitailo, Mod. Phys. Lett. A9 (1994) 1471, hep-ex/9406002.
- [50] S. Sapeta and U.A. Wiedemann, (2008), 0809.4251.
- [51] S. Lupia and W. Ochs, Phys. Lett. B418 (1998) 214, hep-ph/9707393.
- [52] Y.L. Dokshitzer, V.A. Khoze and S. Troian, Int. J. Mod. Phys. A7 (1992) 1875.
- [53] V.A. Khoze, S. Lupia and W. Ochs, Phys.Lett. B386 (1996) 451, hep-ph/9604410.
- [54] S. Albino et al., (2008), 0804.2021.
- [55] S. Albino, Rev. Mod. Phys. 82 (2010) 2489, 0810.4255.
- [56] S. Bethke, Nucl. Phys. Proc. Suppl. 234 (2013) 229, 1210.0325.
- [57] Particle Data Group, J. Beringer et al., Phys.Rev. D86 (2012) 010001.
- [58] D. d'Enterria and R. Pérez-Ramos, Proceeds. Moriond-QCD (2014); arXiv:1408.2865 [hep-ph].